Climate change impacts on the ocean's biological carbon pump in a CMIP6 Earth System Model

Stevie Walker

A Senior Honors Thesis Presented to

Dr. Hilary Palevsky

Department of Earth and Environmental Sciences

Boston College

April 20th, 2021

Abstract

The ocean plays a key role in global carbon cycling, taking up CO_2 from the atmosphere. A fraction of this CO_2 is converted into organic carbon through primary production in the surface ocean and sequestered in the deep ocean through a process known as the biological pump. The ability of the biological pump to sequester carbon away from the atmosphere is influenced by the interaction between the annual cycle of ocean mixed layer depth (MLD), primary production, and ecosystem processes that influence export efficiency. Gravitational sinking of particulate organic carbon (POC) is the largest component of the biological pump and the aspect that is best represented in Earth System Models (ESMs). I use ESM data from CESM2, an ESM participating in the Coupled Model Intercomparison Project Phase 6 (CMIP6), to investigate how a high-emissions climate change scenario will impact POC flux globally and regionally over the 21st century. The model simulates a 4.4% decrease in global POC flux at the 100 m depth horizon, from 7.12 Pg C/yr in the short-term (2014-2034) to 6.81 Pg C/yr in the long-term (2079-2099), indicating that the biological pump will become less efficient overall at sequestering carbon. However, the extent of change varies across the globe, including the largest POC flux declines in the North Atlantic, where the maximum annual MLD is projected to shoal immensely. In the future, a multi-model comparison across ESMs will allow for further analysis on the variability of these changes to the biological pump.

Acknowledgements

Funding for this thesis was provided by the Microsoft AI for Earth Grant.

Hilary - I cannot begin to thank you enough. Your endless support, mentorship, and guidance have been instrumental in making this thesis a reality. No matter how different this project may be from what we first thought way back before COVID-19, you were always there to help and encourage me through it. My perception of who I am, and who I can be, as a scientist is profoundly different because of you. Thank you.

Tara - Thank you for taking me under your wing when I was a freshman. You opened my eyes to the world of scientific research and inspired my love of learning in so many ways. I am very grateful for all of the support and mentorship you have provided me over these past four years.

Hem - Thank you for all of your help with setting up my server and for teaching me the ins-and-outs of cloud computing and R coding. Your advice was instrumental for my methods.

Ben - Thank you for your advice on my thesis figures and for helping me learn to love coding.

Mom - You have been my rock through the past four years (and all the years before that too, obviously), and I am so thankful for all of your help and guidance on my journey through college. Thank you for always believing in me.

Dad - Now, nearly 10 years later, I understand what all of the hours you spent working on your Master's thesis were for. I wish you were here to read mine. I honor you for your gifts and lessons in and of authenticity.

And to all my friends and family who have supported me on my journey at BC, thank you.

Table of Contents

Chapter One: Introduction

1.1 Climate change impacts on the ocean

Anthropogenic climate change, as caused by the burning of fossil fuels and rapid land use change since the start of the Industrial Revolution, poses major threats for the ocean. Warming temperatures, ocean acidification, and ocean deoxygenation are causing cascading impacts for marine biogeochemical cycles and ecosystem dynamics (Bopp et al., 2013; Gruber, 2011). Increasing sea surface temperatures are causing physical changes, such as increased stratification, reduced mixing, increased frequency and intensity of marine heat waves, and decreased carbon dioxide and oxygen gas solubility (Frölicher et al., 2018; Kwiatkowski et al., 2020). These physical and chemical changes also induce changes to marine species and ecosystems, including poleward shifts in species distribution, changes in metabolism, increased physical stress to organisms, and biodiversity declines (Bopp et al., 2013; Doney et al., 2012). Because of increased stratification, the supply of nutrients to the euphotic zone is reduced, leading to global declines in phytoplankton productivity (Behrenfeld et al., 2006). Furthermore, stratification reduces ventilation of the water column, leading to the creation of more hypoxic (low oxygen) and anoxic (no oxygen) areas where organism mortality increases and biogeochemical cycling is altered (Oschlies et al., 2018). The ocean's absorption of CO_2 has helped keep carbon out of the atmosphere, but it is causing ocean acidification - a decline in ocean pH and shifts in seawater carbonate chemistry, which reduces the ability of calcifying organisms to create their shells and survive (Doney et al., 2009). Together, these impacts of anthropogenic climate change have synergistic effects that we are just beginning to understand (Gruber, 2011) and will greatly impact marine ecosystems and the ocean's role in the carbon cycle (Bopp et al., 2013; Kwiatkowski et al., 2020).

1.2 The biological carbon pump

The ocean plays a key role in the carbon cycle as a large carbon sink, absorbing ~30% of anthropogenic carbon emissions (Bopp et al., 2013), or 2.5 ± 0.6 $GtCyr^{-1}$ in the last decade (Friedlingstein et al., 2020). After CO_2 is converted to organic carbon by phytoplankton, a fraction of this organic carbon sinks to the deep ocean and remains out of contact with the atmosphere on a time scale of seasons to centuries - a process known as the biological pump (Le Moigne, 2019; Siegel et al., 2014). Without the biological pump, it is estimated that the CO_2 concentration in the atmosphere would be ~200 ppm higher (Parekh et al., 2006). The biological carbon pump is a highly complex system with many component processes that remain poorly understood and quantified. It functions through three main forms: 1) gravitational flux, or sinking, of particulate organic carbon (POC), 2) downward transport of neutrally buoyant organic carbon via circulation of water masses, and 3) vertical animal migrations, including the seasonal copepod lipid pump and diurnal vertical migration (DVM) by zooplankton and fish that feed at the surface at night and return to the mesopelagic during the day, releasing organic carbon in the form of fecal pellets at depth (Jónasdóttir et al., 2015; Le Moigne, 2019). POC, also known as “marine snow”, is organic carbon that is large or dense enough to sink. It is made up of dead phytoplankton, aggregates of cells, and zooplankton fecal pellets (Le Moigne, 2019). POC differs from dissolved organic carbon (DOC) because DOC is organic carbon that is either dissolved in water or too small to sink. DOC only sinks by physical mixing (Le Moigne, 2019). Both are important components to the total biological pump export (Boyd et al., 2019), though this thesis focuses primarily on POC flux.

1.3 Export and transfer efficiency of the biological pump

The overall strength of the biological pump is influenced by both the rate of primary production in the surface ocean, and by biological and physical influences on the efficiency of organic matter transfer from the surface into the deep ocean. Photosynthesis by phytoplankton in the surface ocean generates organic matter (also referred to in this thesis as organic carbon, marine snow, and POC). The majority of this organic matter is remineralized - i.e. consumed by heterotrophs through respiration - but a fraction sinks out of the surface ocean and into the deep ocean. The deeper POC sinks, the more time it has to be remineralized back into inorganic carbon (dissolved CO_2), leading to POC flux attenuation at depth (Le Moigne 2019). Flux attenuation occurs exponentially in the water column, and has been mathematically modeled in several ways (Cael and Bisson 2018), such as the Martin Curve (Martin et al. 1987). The strength of the biological pump can be influenced by how fast remineralization is occurring, as well as the speed that organic matter sinks (Le Moigne 2019). This affects the export efficiency (e-ratio) of a region, which is the fraction of net primary productivity (NPP) that is exported past a defined depth (Laufkötter et al., 2016; Palevsky & Doney, 2021). E-ratio, as well as POC flux, are impacted by the choice of depth horizon. Common depth horizons used include 100 m, the depth of the euphotic zone, the particle compensation depth, and the maximum annual mixed layer depth (Palevsky and Doney 2018).

A key physical factor that influences the strength of the biological pump is ocean mixed layer depth (MLD). The MLD is the surface layer of the ocean where the water column is well mixed and active exchange is happening with the atmosphere. It is where most of the photosynthesis in the ocean occurs, and it plays an important role in regulating Earth's climate by exchanging heat and carbon with the atmosphere and deep ocean (Sallée et al., 2021). MLD

varies both seasonally and regionally based on the amount of physical mixing; the deepest mixed layers are found in the winter when the most convective mixing occurs, and the MLD shoals in the summer as increasing surface water temperatures stratify the water column (Palevsky & Nicholson, 2018). Understanding the seasonal cycles of ocean MLD is important for understanding the timescales with which carbon is sequestered via the biological pump because carbon must sink below the maximum annual MLD (MLD_{max}) in order to be fully out of contact with the atmosphere and to avoid remineralization- the respiration of organic carbon into CO_2 (Palevsky & Nicholson, 2018). Thus, it is important to evaluate POC flux at the MLD_{max}, as opposed to the 100 m depth horizon that it is typically evaluated at in climate models, because it gives a more accurate picture of how much POC is being sequestered on time-scales longer than a year (Palevsky & Doney, 2021; Palevsky & Doney, 2018). As climate change worsens, the MLD is expected to shoal and the ocean is projected to become more stratified as a whole, leading to reduced air-sea gas exchange, deep ocean ventilation, and biological productivity (Sallée et al., 2021). However, there are still many uncertainties about how intense the impacts of a shallower MLD will be, especially when it comes to complex processes like the biological pump.

1.4 Climate change impacts on the biological carbon pump

Earth system models (ESMs) consistently agree that the strength of the biological carbon pump is projected to decrease as climate change intensifies (Bopp et al. 2013; Cabré et al. 2015; Fu et al. 2016; Laufkötter et al. 2016; Palevsky and Doney 2021), but the magnitude of the change is uncertain, ranging from a 5% to a 20% decrease in POC flux (Laufkötter et al., 2016). Even seemingly small reductions will have large feedbacks on the strength of the global carbon

cycle because carbon is exported to the deep ocean at a higher rate than the surface ocean absorbs carbon dioxide from the atmosphere (Friedlingstein et al., 2020; Palevsky & Doney, 2021). Furthermore, reductions in the efficiency of the biological pump could impact future deep ocean acidification and deoxygenation (Oschlies et al. 2008). Understanding climate change-related impacts on the biological pump requires investigating both physical impacts, such as stratification due to surface ocean warming, and biological impacts, such as NPP changes due to nutrient availability. As stratification increases, there is less mixing between the surface and deep ocean, which has mixed impacts on the biological pump because it reduces surface nutrient supply and subsequent NPP while at the same time preventing deep ocean carbon from being ventilated back into the atmosphere (Fu et al., 2016; Palevsky & Doney, 2021). Globally, NPP is projected to decrease for a variety of reasons (Bopp et al., 2013; Fu et al., 2016), which will reduce the amount of organic carbon available for export via the biological pump.

1.5 Marine biogeochemical modeling's role in analyzing the biological pump

Predicting climate change impacts on the biological pump, as well as understanding how it functions overall, is limited by observational data. As a whole, large scale observations of the biological pump are scarce, especially in remote areas of the ocean that are difficult to reach and make continuous observations in. Our ability to make these observations is improving as technology advances and as more time-series data is collected through projects, such as the Oceans Observatory Initiative (OOI; Smith et al., 2018), the Bermuda Atlantic Time Series (BATS; Steinberg et al., 2001), and the Hawaii Ocean Time Series (HOT; Karl & Lukas, 1996). As a solution to the lack of observational studies, Earth System Models (ESMs) can help us understand how the principles we have found in observations play out in a system where we can

resolve global full-depth data. Understanding how the biological pump functions on a global scale is no easy task, especially when thinking about what synergistic changes will occur in the future as climate change continues. ESMs can also be used to simulate these future changes without us having to wait for them to play out in the real world.

ESMs are computer models that allow us to better understand complex global-scale dynamics by physically simulating processes and interactions of all aspects of Earth's climate system - including land, atmosphere, ocean, ice, and biosphere - under various climate scenarios (Heavens et al., 2013). The ocean biogeochemistry component of ESMs is a powerful tool we have to study the ocean carbon cycle and its response to future changes (Séférian et al., 2020). The latest model advancements allow ESMs to include more complexities and increased nominal resolution (model grid cell size), which is important for more precise regional applications (Hayhoe et al., 2017; Walker et al., 2021). Furthermore, ESMs now include better representation of lower trophic levels with more phytoplankton functional groups, finer-scale physical ocean processes (i.e. mesoscale eddies), variation in stoichiometric ratios, and the parameterization of more micronutrients (Séférian et al., 2020). One more key ESM improvement is that modeling groups that participated in CMIP6 (described in the following section) have made archived depth resolved POC flux data available for the first time (Orr et al. 2017). In the previous version, CMIP5, modeling groups were only asked to archive POC flux data at the 100 m depth horizon. Having POC flux data archived at all depths enables more complex analysis of influences on the biological pump, such as that of MLD_{max}, and was a major motivating factor for the types of analyses I performed in this thesis.

1.6 Coupled Model Intercomparison Project Phase 6 (CMIP6)

All data in this thesis come from models that are a part of the Coupled Model Intercomparison Project Phase 6 (CMIP6), an internationally coordinated effort to provide open-access data from the world's most advanced General Circulation Models (GCMs; see section 2.1) and ESMs (Eyring et al., 2016). CMIP6 provides climate change projections for a variety of fossil fuel emissions and land use scenarios, including future climate and paleoclimate (Juckes et al., 2020; O'Neill et al., 2016). CMIP was started over 20 years ago, and has since grown into a complex project made up of 23 independently-led, CMIP-endorsed model intercomparison projects (MIPs), each with their own specialized research questions and focus (Juckes et al., 2020). Predictions from CMIP are used to inform the Intergovernmental Panel on Climate Change's (IPCC) global synthesis reports, such as the upcoming sixth assessment report (AR6), which will help create mitigation and adaptation strategies for future climate change. As a whole, CMIP6 models predict greater ocean warming, acidification, and deoxygenation, but less net primary productivity declines than CMIP5 - the previous version of CMIP (Kwiatkowski et al., 2020). One more key ESM improvement in CMIP6 is that modeling groups have made archived depth resolved POC flux data available for the first time (Orr et al. 2017). In the previous version, CMIP5, modeling groups were only asked to archive POC flux data at the 100 m depth horizon. Having POC flux data archived at all depths enables more complex analysis of influences on the biological pump, such as that of MLD_{max}, and was a major motivating factor for the types of analysis I performed in this thesis. CMIP6 is made up of the most advanced ESMs available today and includes improvements from CMIP5 ESMs that have directly enabled analysis of depth-related characteristics of the biological pump.

1.7 Purpose and objectives

This thesis aims to investigate how carbon sequestration via the biological pump is expected to change under a high-emissions scenario on both global and regional scales. I analyze data from one CMIP6 model, the Community Earth System Model version 2.0 (CESM2; Danabasoglu et al., 2020) to view spatial changes in the flux of particulate organic carbon (POC) from the surface to the deep ocean, spatial changes in ocean MLD, as well as depth-resolved POC flux changes in four high-latitude regions, one subtropical region, and one equatorial region. The two questions that best frame my analysis are: 1) How is the flux of POC expected to change under a high emissions scenario? and 2) What areas of the ocean will see the greatest change in POC flux? Many of the analyses in this study are in line with Palevsky and Doney (2021), which used data from CESM1, the previous version of CESM2 that was used in CMIP5, allowing me to cross compare differences in projections between model comparison projects.

Chapter 2: Methods

2.1 CMIP6 and ScenarioMIP

The data in this study come from the Coupled Model Intercomparison Project Phase 6 (CMIP6): the world's leading international multimodel research project (Eyring et al., 2016). Modeling centers from all across the globe have Earth System Models (ESMs) and General Circulation Models (GCMs) that have been included in CMIP6, each with their own mathematical configurations and variables. ESMs are computer models based on fundamental equations of physics that are dynamically linked to include interactions between different parts of the Earth system (i.e. land, ocean, atmosphere, biosphere, cryosphere, ocean biogeochemistry), as well as how key variables (i.e. carbon, heat, etc.) travel through each component of the Earth system (Eyring et al., 2016; Heavens et al., 2013). They include more variables and are more complex than GCMs (Heavens et al., 2013), but both types of models have the same goal: to understand how Earth's climate system functions. In order to ensure each ESM is following the same basic guidelines, CMIP6 requires each modeling group to run a set of common experiments, known as the Diagnostic, Evaluation and Characterization of Klima (DECK) experiments (Eyring et al., 2016). All data produced by the ESMs are standardized and publicly available on the Earth System Grid Federation website (https://esgf-node.llnl.gov/). CMIP has many applications, including informing the climate change projections used in the IPCC's global reports, as well as regional analysis.

Compared to CMIP5, the previous release of CMIP model data, CMIP6 builds upon climate modeling advances made in CMIP5 by introducing a new set of future emission scenarios, the Scenario Model Intercomparison Project (ScenarioMIP). The main advancement in

ScenarioMIP is the development of five new shared socioeconomic pathways (SSPs) that examine the interactions between physical climate change and global socioeconomic outcomes (O'Neill et al., 2016; Tebaldi et al., 2020). SSPs have improved upon their CMIP5 equivalent, the Representative Concentration Pathways (RCPs), by including both the change in radiative forcing (W/m^2) described in the RCPs and different societal outcomes in the 21st century. Each SSP describes a possible trend in the development of society and ecosystems over the 21st century, including varying strategies of adaptation and mitigation against climate change: SSP1 - sustainability, SSP2 - middle of the road, SSP3 - regional rivalry, SSP4 - inequality, and SSP5 - fossil-fueled development (O'Neill et al., 2014; Riahi et al., 2017). In my thesis, I focus on scenario SSP5-8.5 because it is the scenario with the largest increase in radiative forcing and the most unsustainable societal outcome: economic and social development supported by the exploitation of fossil fuels, and energy and resource intensive lifestyles that become prominent all around the world (Riahi et al., 2017). As a result of fossil-fuel dependence, SSP5-8.5 has the highest carbon emissions and land use changes, leading to the most intense climate change outcomes over the 21st century.

Aside from the reformatted climate change scenarios in ScenarioMIP, CMIP6 ESMs have become more advanced and complex, especially in improvements made to biogeochemical modeling - both in the land and ocean model components. The majority of models have improved their horizontal nominal resolution, the size of the model grid cells, by using a finer resolution (typically 100km) (Kwiatkowski et al., 2020; Séférian et al., 2020). Changes in ocean models are particularly relevant because this ESM model component contains variables that will impact model results related to POC flux and the ocean's biological pump overall, such as MLD. One such relevant change is improvements in vertical ocean model grid resolution, which allows

models to better represent physical processes throughout the water column, such as stratification and the sinking of organic matter, two key processes I am analyzing in this thesis. In terms of their ocean model components, many CMIP6 ESMs have been updated to include more elements of biogeochemical cycling. 8 out of 12 models have upgraded their ocean models, including improved representation of dissolved oxygen, plankton functional types, micronutrients, and variable stoichiometric ratios (Séférian et al., 2020).

2.2 Model Selection

Earth System Models were selected based on data availability. I developed the following model criteria and used the Earth System Grid Federation search engine (https://esgf-node.llnl.gov/search/cmip6/) to find which models met my search criteria. 1) The model participated in ScenarioMIP and ran SSP5-8.5. 2) The model ran and archived the following variables related to understanding the biological carbon pump: particulate organic carbon flux (mol m^{-2} yr^{-1}) at all depths throughout the water column (expc), particulate organic carbon flux (mol m^{-2} yr^{-1}) specifically at the 100 meter depth horizon (epc100), ocean mixed layer depth (m) (mlotst), and net primary production (pp or ppos). 3) All the data needed were available for download.

From these criteria, four different models qualified for use: CESM2, GFDL-ESM2, MPI-ESM1-2, and UKESM1-0-LL (Table 1). The IPSL-CM6A model met criteria 1 and 2, but the data were not available at the time of evaluation. Completing a multi-model comparison with these five models would allow me to identify uncertainty due to internal model variability and differing parameterizations between models (Semenov & Stratonovitch, 2010). However, doing a multi-model comparison is much more complex than analyzing data from just one model, and

ultimately I decided a multi-model comparison was too large of a scope for this thesis. Thus, I moved forward by selecting the Community Earth System Model (CESM2; Danabasoglu et al., 2020) for analysis. CESM2 was chosen because Palevsky & Doney (2021) completed a similar analysis with CESM1 (Gent et al., 2011; Hurrell et al., 2013), the CMIP5 version of CESM, which enables the ability to cross compare between CMIP5 and CMIP6 results.

Earth System Model (ESM)	Modeling Group	Ocean Grid Resolution (km)	Reference	Ocean Model	Marine Biogeochemistry Model
CESM2	National Center for Atmospheric Research	100	(Danabasoglu et al., 2020)	POP2	MARBL
GFDL-ESM2M	Geophysical Fluid Dynamics Laboratory	55	(Dunne, 2019)	MOM6	COBALTv2
MPI-ESM1-2-HR	Max-Planck-Institut für Meteorologie	45	(Gutjahr et al., 2019)	MPI-OM	HAMOCC5
IPSL-CM6A-LR	Institut Pierre‑Simon Laplace	100	(Boucher et al., 2020)	NEMO-OPA	NEMO‑PISCES
UKESM1-0-LL	UK Earth System Modeling Project	100	(Sellar et al., 2019)	NEMO v3.6,-CICE	MEDUSA-2.0

Table 1. *Description of Earth System Models that met the majority of search criteria, including which modeling group constructed the model, the size of each model's grid cells, the name of the ocean component of the ESM, and the name of the marine biogeochemistry component of the ESM.*

2.3 Model Description

The Community Earth System Model (CESM2) is a fully-coupled ESM that comprehensively models interactions between the atmosphere, land, ocean, and sea-ice (Danabasoglu et al., 2020). Similar to many other ESMs in CMIP6, it has a nominal 1° (~100km) grid resolution. Grid cells in the model are evenly spaced in the zonal direction, but are unevenly spaced in the meridional direction. Additionally, the North Pole is displaced into Greenland, but the Southern hemisphere uses spherical coordinates (Danabasoglu et al., 2020), making the

CESM2 native grid appear slightly distorted compared to a standard map projection (Figure 1). The ocean component of CESM2, Parallel Ocean Program version 2 (POP2; Smith et al., 2010), is the same as CESM1, except it has numerical improvements in physical mixing and more advanced parameterizations. The ocean biogeochemistry model component, Marine Biogeochemistry Library (MARBL), is an updated version of the Biogeochemistry Elemental Cycle model (BEC; Moore et al., 2004) used in CESM1. It includes Fe, O_2, Si, P, N, and C in its nutrient cycling component, simulates sinking particulate organic matter implicitly, has three explicit phytoplankton functional groups (diatoms, diazotrophs, and pico/nano phytoplankton), one implicit phytoplankton functional group (calcifiers), and one zooplankton functional group (Danabasoglu et al., 2020; Séférian et al., 2020). The vertical grid points are not evenly spaced; the CESM water column has a vertical resolution of 10 m up to a depth of 160 m, followed by a decreasing resolution of up to 250 m all the way down to the model's maximum depth of 5,500 m (Danabasoglu et al., 2020).

It is important to note that all spatial analysis was calculated on the CESM2 native grid to ensure internal consistency in my calculations. Thus, when I refer to latitude and longitude in my figures, it refers to approximated values based on the CESM native grid (Figure 1), not actual map coordinates. This is also why all of the global figures found in this thesis do not have traditional map coordinates (i.e. °N,°S,°E,°W).

a)

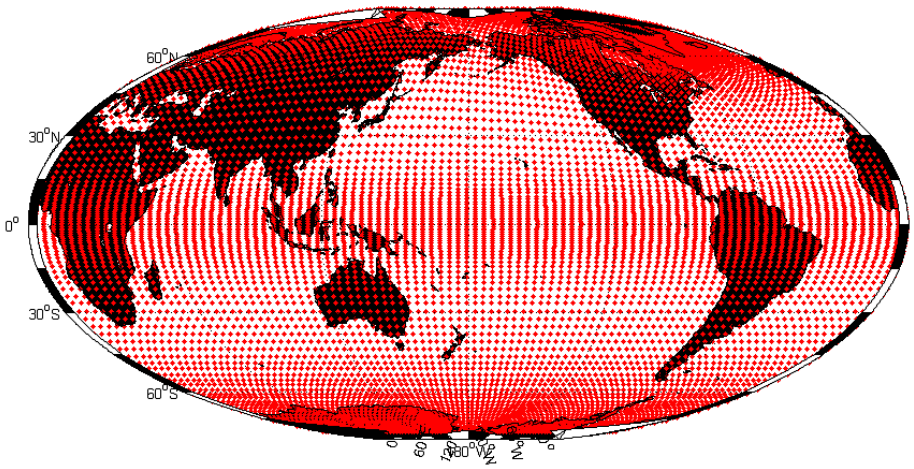

b)

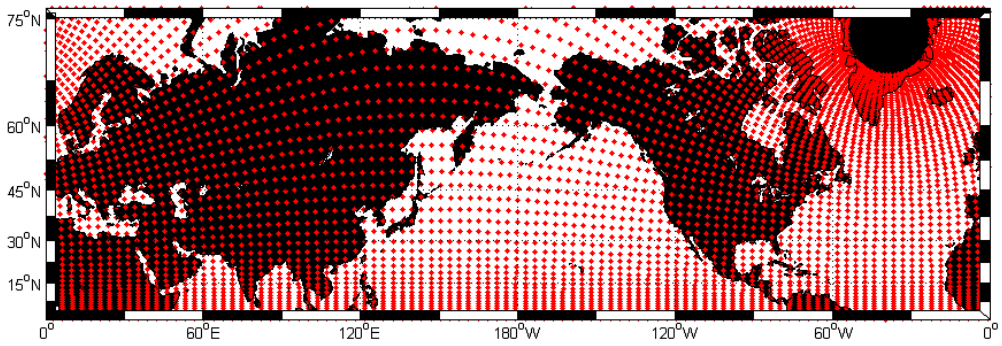

Figure 1. *CESM native grid. Each red dot represents one model grid cell. a) Global map projection b) Northern-hemisphere mercator projection, showing the offset of the North Pole over Greenland. Source: Hilary Palevsky.*

2.4 Microsoft Azure Server Set-up

All data downloading and analysis were performed using a Linux server running Rstudio. The R code written for this thesis is available at the following Github repository: https://github.com/steviewalker/senior_thesis. Using Microsoft Azure, Microsoft's cloud computing service (Copeland et al., 2015), I built a virtual machine to be able to process large amounts of ESM data. The main benefits of using cloud computing are increased computational

capacity, high-speed data downloading using Microsoft's WiFi, and unlimited amounts of storage in the Azure cloud (Copeland et al., 2015). First, I created the virtual machine in the Azure portal, and then I configured it using code from Morzaria-Luna (2020). I created and attached a one terabyte data disk to my virtual machine for storing ESM data. Virtual machines can be resized based on computational capacity needs; for most data analysis completed, I used the standard D4s_v3 size (vCPUs: 4, RAM: 16GiB, max IOPS: 6400, temporary storage: 32 GiB).

2.5 Data acquisition and formatting

After setting up the server, I used the wget utility to download data from the ESGF web server. Wget is a command utility used to download files from various web servers. In order to organize and obtain wget download links from the ESGF website, I used the epwshiftr package (Jia & Chong, 2021), storing the links in a file index. However, for unknown reasons, the epwshiftr package did not work for every ESM. For the models it missed, I manually generated a file index using Microsoft Excel. My initial download of data from five different ESMs was approximately 240 gigabytes. All the data downloaded were in the format of network common data form (NetCDF) files, a data abstraction meant for storing multidimensional scientific data (Rew & Davis, 1990).

The raw CESM data was divided into two chunks based on the year, in order to make each file smaller and thus, easier to download from the ESGF database. However, since I was not limited by computational capacity, it was more convenient for me to combine all the files from each variable into a single file. I used modified code from Walker (2020) to combine the CESM files. CESM also had data from multiple ensemble members, but for simplicity's sake, I chose just one ensemble member, r10i1p1f1, for further analysis.

2.6 Global Data Analysis

First, I collected all the file metadata from the combined CESM files. This allowed me to understand how each variable is included in the NetCDF file and what the dimensions of each file are. For example, the epc100 NetCDF file, particulate organic carbon (POC) flux at 100 m depth, has three dimensions: latitude, longitude, and time. Next, I calculated average POC flux at 100 m for the entire globe (i.e. for each model grid cell) in a short-term 20 year climatological mean (2014-2034) and a long-term 20 year climatological mean (2079-2099). I chose to calculate short-term and long-term climatological means because this smooths out interannual variability, making the long-term patterns at the beginning and end of the 21st century clear. I also calculated the change in average POC flux at 100 m (long-term minus short-term), allowing me to evaluate the modeled outcomes of worst-case-scenario climate change over the 21st century.

The next step in my analysis was to calculate the average maximum annual mixed layer depth (MLD_{max}). Here, the MLD_{max} was chosen rather than a different depth horizon because below this depth, POC is considered fully sequestered away from contact with the atmosphere. For example, convective winter mixing causes the mixed layer to deepen, ventilating it and allowing POC to be remineralized instead of being sequestered on longer time-scales, which makes MLD_{max} an appropriate choice for the depth horizon (Palevsky & Doney, 2018). First, I calculated the maximum annual MLD at each grid cell for each calendar year for 20 years in the short-term (2014-2034) and 20 years in the long-term (2079-2099). I then took the average over the two 20 year periods to smooth out interannual variability. The final output was a matrix with

a single MLD_{max} value for each latitude and longitude. I subtracted the long-term average MLD_{max} from the short-term average MLD_{max} to find the change in MLD_{max}.

2.7 Regional Data Analysis

For my regional analysis, I calculated depth profiles from the more complex, depth-resolved POC flux data, the expc NetCDF file, which includes four dimensions: latitude, longitude, depth, and time. I selected six map points to analyze depth resolved POC flux (Figure 2): the Labrador Sea (a), Iceland Basin (b), Equatorial Eastern Pacific (c), Subtropical North Pacific (d), Southern Ocean (e), and Bellingshausen Sea (f). I chose four high-latitude regions because these are the regions where climate change impacts such as increased stratification and changes in NPP are expected to be the strongest. More specifically, I chose the Labrador Sea and Iceland Basin because it is a region where the MLD is projected to shoal extensively over the 21st century (Palevsky & Doney, 2021), and I chose the Southern Ocean and Bellingshausen Sea because NPP is expected to increase in these regions (Cabré et al., 2015; Laufkötter et al., 2015). I chose one equatorial region and one subtropical region to see any contrasts based on latitude. Additionally, the Equatorial Eastern Pacific is a region of high NPP, so this region was also chosen to see if there were any POC flux changes due to declines in nutrient delivery to the surface ocean from increased stratification (Cabré et al., 2015). From these six points, I calculated the average POC flux in the short-term (2014-2034) and in the long-term (2079-2099) at each of the 60 depths included in the model. This allowed me to generate depth profiles for each location. The climatological MLD_{max} for both the short-term and long-term was also included in each depth profile.

The second component of my regional analysis was looking at POC flux changes between the short and long-term through two latitudinal transects, one along the Atlantic and one along the Pacific (Figure 2). This involved calculating average POC flux in the short-term (2014-2034) and in the long-term (2079-2099) at each depth and latitude along one chosen longitude. Longitude was selected to include the most latitude grid cells with values (i.e. the most continuous length of ocean). Looking at a transect allows us to see if there are any common latitudinal patterns in POC flux change. Because the transects were made using the model's native grid, high Southern latitudes are indicated by low grid cell values (~0-50) and high latitude Northern latitudes are indicated by high grid cell values (~330-380).

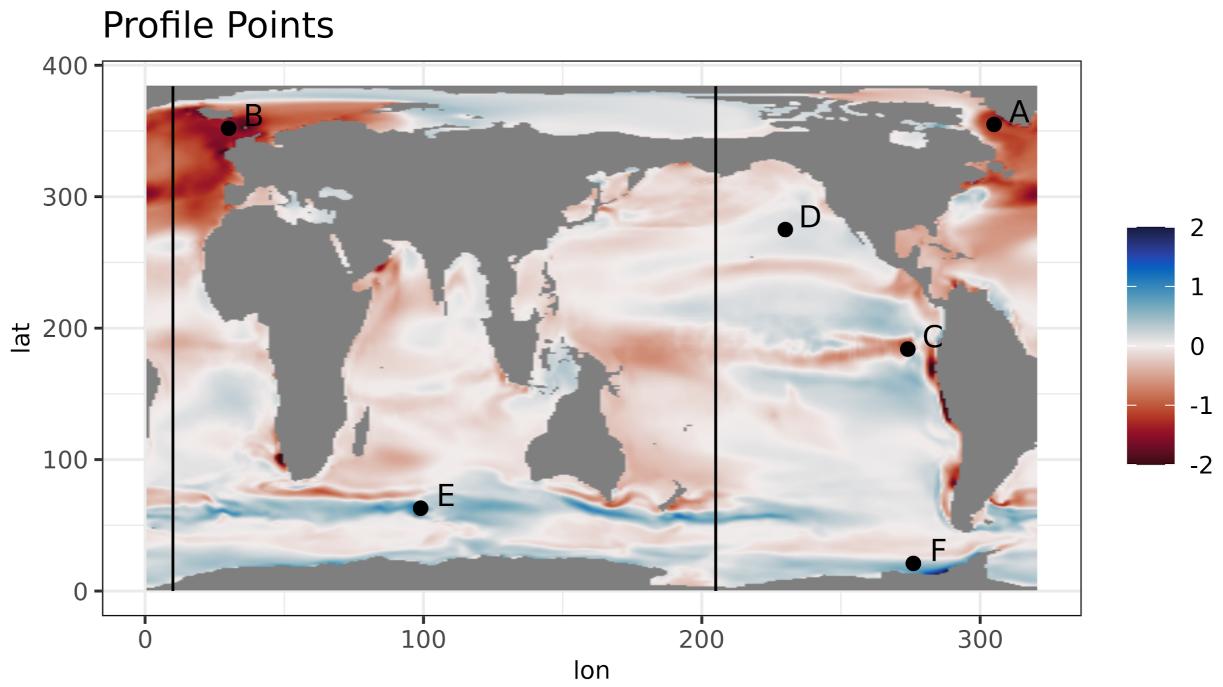

Figure 2. *Location of POC flux depth profiles and POC flux transects, plotted over Figure 3c, change in POC flux (mol m^{-2} yr^{-1}) over the 21st century. The lettering of each point corresponds with the depth profile in Figure 5. The vertical lines indicate the location of the POC flux transects in Figures 6-9.*

Chapter 3: Results and Discussion

I begin with a global-scale analysis of CESM2 data by reproducing past CMIP5 model analyses (Cabré et al. 2015; Fu et al. 2016; Laufkötter et al. 2016; Palevsky and Doney 2021) but with the newest version of CESM from CMIP6. I analyze modeled POC flux at the 100 m depth horizon because this is the depth horizon the majority of past literature has used to look at POC flux in model simulations. The second component of my global analysis investigates changes in stratification (MLD_{max}) over the 21st century. Past studies have completed this analysis using CMIP5 models, namely Palevsky and Doney (2018 and 2021), which both recognized the importance of using MLD_{max} as a depth horizon for calculating POC flux because POC that makes it below the MLD_{max} is sequestered long-term. Thus, the 100 m depth horizon does not give the whole picture of how POC flux is going to change because POC flux will be regionally affected by stratification.

The second main section of my results presents a regional analysis of POC flux changes in CESM2, illustrating the power of having depth-resolved model output to look at POC flux change not only at 100 m, but throughout the full water column. This shows the interactions between changes in POC flux and MLD_{max}. I begin my regional analysis with six depth profile plots at specific stations of interest, illustrating the range of conditions found globally (see section 2.7 for a justification of depth profile point selection). I also present latitudinal transects of POC flux in the Atlantic and Pacific, allowing for cross comparisons of depth resolved changes in different ocean basins, as well as visualizations of latitudinal trends in POC flux change.

3.1 Change in POC flux at the 100 m depth horizon over the 21st century

I first present POC flux at 100 m because this is the depth horizon that has been most commonly used to assess POC flux and its change under climate change scenarios in past model analyses. Spatial trends in POC flux remain similar throughout the 21st century simulation, as presented in climatological mean POC flux over both the short-term (2014-2034) and the long-term (2079-2099) 20 year periods evaluated (Figure 3a and b). POC flux is the highest in the Equatorial Pacific and off the west coast of South Africa (Figure 3a and b). This is because these areas are upwelling regions, where nutrients needed for photosynthesis are brought up from the deep ocean and fuel high levels of primary productivity (Cabré et al., 2015). POC flux is generally lowest in the subtropical ocean gyres and in the Southern Ocean (Figure 3a and b), both regions that are nutrient-limited and have lower primary productivity.

Despite the similar overall spatial trends throughout the simulation (Figure 3a and b), there is significant spatial variability in the change in POC flux (Figure 3c). The region with the most widespread and severe POC flux decline is the North Atlantic. Here, increased stratification leads to subsequent declines in convective mixing, reducing the supply of nutrients from North Atlantic deep waters to the surface (Moore et al., 2013; Palevsky & Doney, 2021; Sallée et al., 2021), which could be leading to NPP declines. Understanding the interaction between stratification and productivity declines on POC flux will require analysis of additional model variables, such as NPP and e-ratio (Palevsky & Doney, 2021). Changes in POC flux are generally of a lower magnitude in subtropical and tropical latitudes. The region with the highest levels of POC flux increase is the Southern Ocean (Figure 3c). This increase could be caused by projected increases in Southern Ocean primary productivity (Cabré et al., 2015; Laufkötter et al., 2015), as well as be related to a predicted increase in strength and poleward shift of winds that

drive upwelling in the Southern Ocean (Fu et al., 2016). However, it is important to note that the magnitude of POC flux is lower in the Southern Ocean compared to regions of POC flux decline, such as the Equatorial Pacific and Northern Atlantic (Figure 3), resulting in an overall net global POC flux decline.

Globally, the CESM2 model predicts a 4.4% decline in annual POC flux under SSP5-8.5 over the 21st century, from 7.1 to 6.8 Pg C yr^{-1}. This decline in POC flux is in line with results from the CMIP5 version of CESM2 (CESM1), however the magnitude of decline is lower in CESM2 than CESM1, which predicted an 8.6% decline (Palevsky & Doney, 2021). Changes in POC flux could be due to changes in NPP and/or in the e-ratio - the fraction of NPP that is exported (Laufkötter et al. 2016). Since multiple aspects of the marine biogeochemistry component were updated in CESM2, from BEC to MARBL (Table 1), and since ocean model physics have also been updated (Danabasoglu et al. 2020), there are multiple possible explanations for the difference in overall magnitude of decline between the two model versions. More generally, this decline could also be linked to the trend of NPP declines being less pronounced in CMIP6 than CMIP5 models (Kwiatkowski et al., 2020). Globally integrated CESM2 POC flux results are on the low end of modeled predictions compared to CMIP5 model results, which predicted anywhere between a 1% to 18% decline in global POC flux at 100 m (Bopp et al., 2013; Cabré et al., 2015; Fu et al., 2016; Laufkötter et al., 2016).

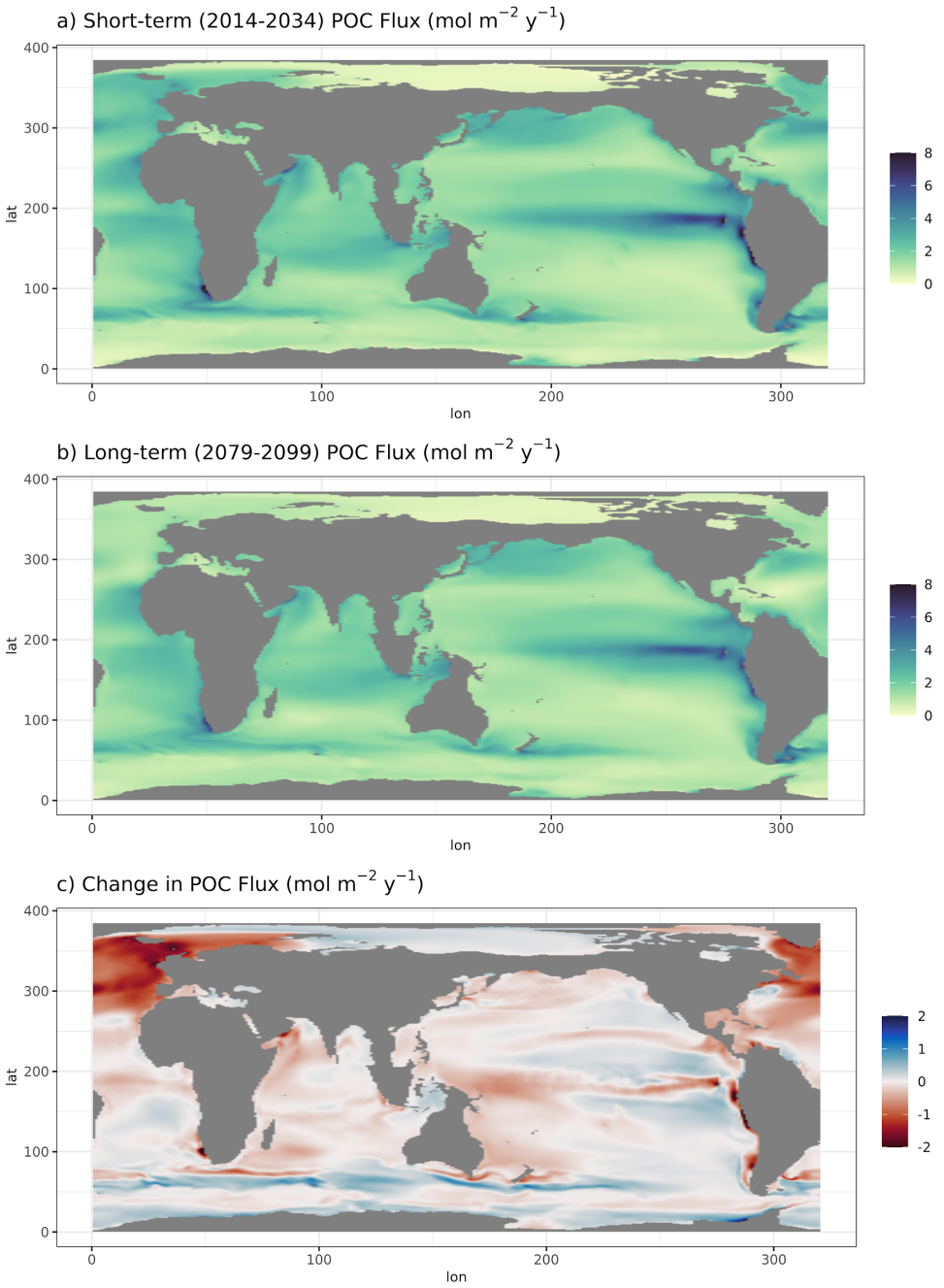

Figure 3. *CESM2 modeled POC flux at the 100 meter depth horizon for the SSP5-8.5 high-emissions scenario. a) Short-term (beginning of the 21st century simulation) climatological mean annual POC flux over the years 2014-2034. b) Long-term (end of the 21st century simulation) climatological mean annual POC flux over the years 2079-2099. c) Change in annual POC flux at the 100 m depth horizon over the 21st century simulation (difference between the short and long term results in panels a and b). Note, the maps are plotted on the CESM2 native grid, resulting in the irregularly shaped continents and non-realistic map coordinates. All gray spaces are model grid cells outside the spatial domain of the marine biogeochemical model component.*

3.2 Change in maximum annual mixed layer depth over the 21st century

Understanding the causes of global POC flux decline requires examining both biological and physical components of the biological pump, such as changes in ocean mixed layer depth. In line with other modeling studies (Kwiatkowski et al., 2020; Laufkötter et al., 2016; Palevsky & Doney, 2021), CESM2 predicts a global shoaling of maximum annual MLD (MLD_{max}) under a high-emissions climate change scenario (Figure 4c). Climatological MLD_{max} in the short-term (2014-2034) is in line with current observations of MLD, with the deepest MLD_{max} values of over 1000 m occurring in the North Atlantic, and deep values around 400 m also occurring in the Southern Ocean (Figure 4a). The shallowest MLD_{max} values occur in the equatorial ocean, where sea surface temperatures are warmer and the water column is more stratified.

As climate change worsens, ocean mixed layer depth will continue to shoal globally due primarily to ocean surface warming and in some regions, such as the North Atlantic, surface freshening because of melting sea ice (Bopp et al. 2001; Fu et al. 2016). A more stratified ocean inhibits the upwelling of nutrients from the deep ocean, leading to primary productivity declines and reduced efficiency of the biological pump through POC flux declines. However, a more stratified ocean reduces the depth that POC has to sink past in order to be sequestered away from the atmosphere on longer time scales (Palevsky & Doney, 2021). Thus, changes in MLD_{max} can have both positive and negative influences on the biological pump depending on which component, biological (NPP) or physical (MLD), is more important in a given region. Calculating POC flux at only the 100 m depth horizon does not capture the full picture of climate change influences on the biological pump because many depths below 100 m are still part of the mixed layer, where some POC is being remineralized rather than sequestered (Palevsky et al. 2016). Evaluating POC flux at multiple depth horizons, like the MLD_{max}, includes the influence

of winter ventilation on POC flux, leading to more realistic predictions of global POC flux change at the MLD_{max} depth horizon (Palevsky and Doney 2021). POC flux can be better understood when looking at patterns throughout the entire water column, which is a key benefit of increased depth-resolved POC flux data availability in CMIP6 models.

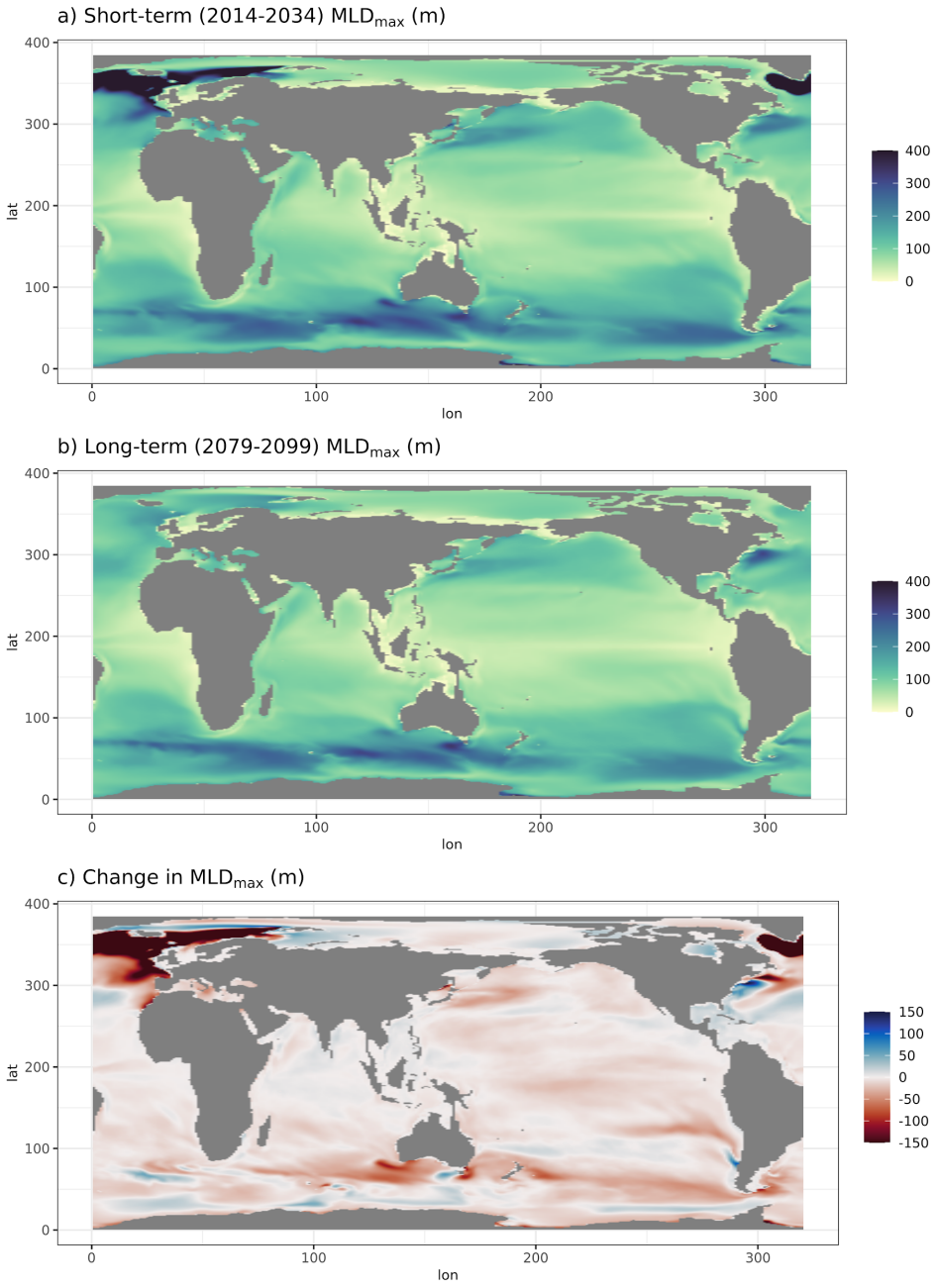

Figure 4. *CESM2 modeled POC flux at the 100 meter depth horizon for the SSP5-8.5 high-emissions scenario. a) Short-term (beginning of the 21st century simulation) climatological mean annual MLD_{max} over the years 2014-2034. b) Long-term (end of the 21st century simulation) climatological mean annual MLD_{max} over the years 2079-2099. c) Change in annual MLD_{max} over the 21st century simulation (difference between the short and long term results in panels a and b). Note, the maps are plotted on the CESM2 native grid, resulting in the irregularly shaped continents and non-realistic map coordinates. All gray spaces are model grid cells outside the spatial domain of the marine biogeochemical model component.*

3.3 Depth-resolved variations in POC flux change over the 21st century

Given the strong regional variations in changes in POC flux (Figure 3c) and MLD_{max} (Figure 4c), depth-resolved analysis of CESM2 model data allows for greater insights into regional climate change impacts on the water column. Using depth resolved POC data, I analyzed results from individual grid cells at points a through f in Figure 2 and latitudinal transects in the Pacific and Atlantic Oceans, as indicated by the lines in Figure 2.

3.3a Depth profiles

The first component of regional analysis are the six depth profiles of POC flux (Figure 5). Each profile shows an increase in POC flux with depth in the surface ocean, where photosynthesis generates organic carbon, followed by a peak at the particle compensation depth, which is the depth where maximum POC flux occurs. At the particle compensation depth, the amount of photosynthesis that is occurring is equal to the amount of respiration. Below the particle compensation depth, respiration exceeds photosynthesis, and the depth profiles resemble the typically observed depth profile of sinking POC flux attenuation, where POC gradually declines as remineralization occurs at depth (Cael and Bisson 2018; Marsay et al. 2015).

Of the six depth profile locations analyzed, locations a and b were chosen because they are from areas where there is a strong decline over the 21st century in POC flux at 100 m (Figure 3). Locations c and d were chosen because they are two non-polar regions with more mild POC flux change signals. Locations e and f were chosen because they are two regions with strong signals of POC flux increase. In the Labrador Sea (Figure 5a, Table 2), there is a 58.4% decline in maximum POC flux over the 21st century. The decline in POC flux can be seen throughout the entire curve except for below depths of about 2000 m. Similarly, in the Iceland Basin (Figure 5b,

Table 2), there is a 58.6% decline in maximum POC flux. Declines are seen throughout the entire depth profile curve, but since the Iceland Basin point doesn't extend below 2000 m, this is not necessarily a direct contrast to the Labrador Sea depth profile. Locations a and b also have the largest shoaling of the MLD_{max} out of the profile points chosen because of freshening in the North Atlantic, consistent with a decline in nutrient supply to the surface ocean, which could have contributed to the decrease in POC flux.

Even though the POC flux decreases over the 21st century in the Labrador Sea and Iceland Basin depth profiles, the transfer efficiency to depth increases, meaning a greater percent of the maximum POC flux is exported past the depth horizons of 100 m, 500 m, and 1000 m (Table 2). In other words, the percent of the POC flux through the particle compensation depth that reaches the deeper depth horizons increases between the short-term and the long-term (Table 2). It is important to note that the results of percent export at the given depth horizons would be different if curves were normalized at 100 m because the flux attenuation above 100 m is very different between the short-term and the long-term results (Table 2). Increasing transfer efficiency to depth is important because deeper remineralization depths lead to longer-term carbon sequestration. Transfer efficiency through the water column is influenced by the interactions between the particles' sinking rate and the rate of respiration consuming the particles; changes between the short-term and the long-term depth profiles are the result of changes in one of both of these factors.

In the Equatorial East Pacific (Figure 5c), POC flux is of a much greater magnitude than any other depth profile analyzed, with a maximum POC flux of 12.68 mol m^{-2} yr^{-1} (Table 2). There is a 24.5% decline in maximum POC flux between the beginning and end of the 21st century in the Equatorial East Pacific, but it is important to note that fractional changes in

locations such as this one, with the highest absolute magnitude of flux at the beginning of the century, will have a disproportionately large effect on globally integrated changes. Furthermore, the absolute fluxes at depth (Table 2) are larger in the Equatorial East Pacific than any other region analyzed, leading to large amounts of carbon sequestration in this region.

In the Subtropical North Pacific, there is comparatively less change in the depth profile curve than other points (Figure 5d). There is a 7.4% increase in maximum POC flux over the 21st century, which is a smaller change than the other depth profile points highlighted here. Compared to the Equatorial East Pacific, this region has very low POC flux overall (Figure 3a and b), which is because ocean gyres are nutrient limited and host less primary productivity (Cabré et al. 2015; Laufkötter et al. 2016). Locations similar to the Subtropical North Pacific, with lower POC flux from the surface but higher transfer efficiency to depth, are places where we might underestimate their role in carbon sequestration if we were only looking at the flux at 100 m, which reflects the importances of depth-resolved analysis.

In the two regions in the Southern Ocean (Figure 5e and 5f), POC flux increases despite slight MLD_{max} shoaling. In point e) Southern Ocean, there is a 71% increase in maximum POC flux, which is most likely related to increases in NPP in this region (Cabré et al., 2015; Laufkötter et al., 2015). Similarly, the 46% increase in maximum POC flux in the Bellingshausen Sea (Table 2) is likely related to the same reason. Depending on the extent of MLD_{max} shoaling in the Southern Ocean, the POC flux increases could contribute positively to long-term carbon sequestration in the region, offsetting some of the decreases in POC flux from other regions that contribute to the overall globally integrated decrease in POC flux in this simulation.

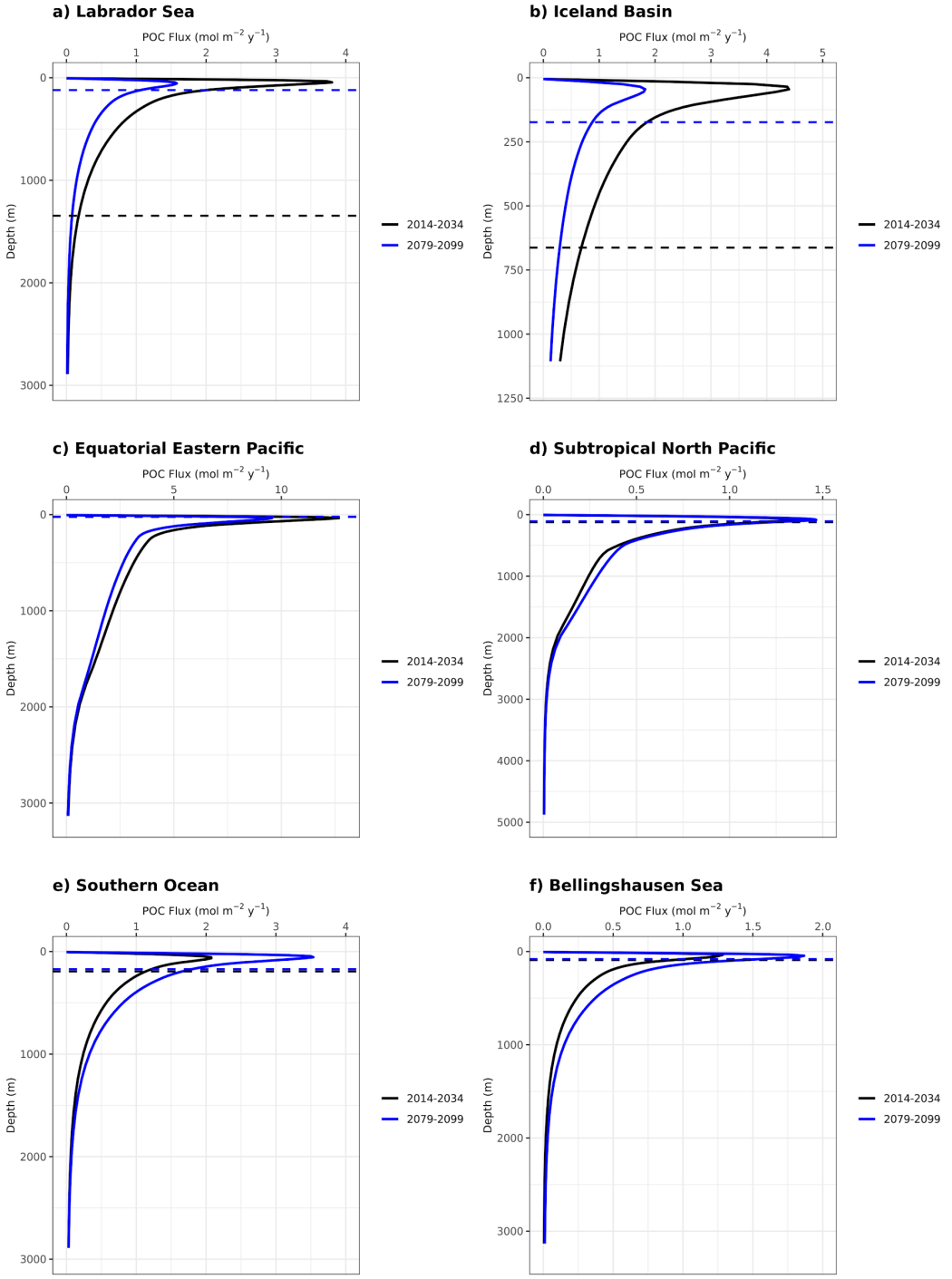

Figure 5. *POC flux depth profiles at select locations in the CESM model. The dotted lines indicate the climatological mean MLD_{max} at the beginning of the 21st century (2014-2034), in black, and the end of the 21st century (2079-2099), in blue. The solid lines represent the short-term and long-term climatological mean annual POC flux. Note: both the x and y axes differ between panels due to different maximum POC fluxes and maximum depths in each location. See Figure 2 for the exact locations of the depth profiles.*

Location	Term	Max Annual MLD (m)	Particle Compensation Depth (m)	Max POC Flux (mol m^{-2} y^{-1})	Flux at 100 m (mol m^{-2} y^{-1})	Flux at 500 m (mol m^{-2} y^{-1})	Flux at 1000 m (mol m^{-2} y^{-1})	POC Flux at 100 m (%)	POC Flux at 500 m (%)	POC Flux at 1000 m (%)
a) Labrador Sea	short-term (2014-2034)	1346	45	3.80	2.26	0.69	0.32	59.4	18.1	8.4
	long-term (2079-2099)	120	55	1.58	1.18	0.34	0.15	74.7	21.7	9.5
b) Iceland Basin	short-term (2014-2034)	663	45	4.40	2.70	0.87	0.37	61.5	19.8	8.5
	long-term (2079-2099)	173	45	1.82	1.23	0.38	0.16	67.7	20.8	8.9
c) Equatorial East Pacific	short-term (2014-2034)	23	35	12.68	7.07	3.07	2.19	55.8	24.2	17.3
	long-term (2079-2099)	21	35	9.57	5.66	2.59	1.85	59.2	27.1	19.3
d) Subtropical North Pacific	short-term (2014-2034)	123	85	1.36	1.27	0.38	0.25	93.1	28.0	18.1
	long-term (2079-2099)	108	85	1.46	1.35	0.42	0.29	92.5	28.5	20.0
e) Southern Ocean	short-term (2014-2034)	194	65	2.07	1.65	0.54	0.25	79.8	26.1	11.9
	long-term (2079-2099)	172	55	3.54	2.55	0.77	0.34	72.0	21.8	9.6
f) Bellingshausen Sea	short-term (2014-2034)	80	35	0.68	0.81	0.23	0.10	63.2	17.7	7.6
	long-term (2079-2099)	64	35	2.31	1.25	0.35	0.15	67.0	18.9	8.2

Table 2. *Characteristics of the depth profile locations shown in Figure 2. Annual MLD_{max} refers to the average annual maximum mixed layer depth. Particle compensation depth is where the maximum POC flux (mol m^{-2} y^{-1}) occurs. The last three columns show the percent of POC flux at the specified depths that is occurring in relation to the maximum POC flux (ex. POC flux at 100 m / maximum POC flux x 100%).*

3.3b Latitudinal transects

Depth-resolved POC flux changes across latitudes helps put the depth profile results into a broader spatial context. Looking at transects in the Atlantic and Pacific Ocean, the vertical lines in Figure 2, allows us to see latitudinal differences in POC flux throughout the entire water column. In all transect figures (Figures 6-9), the left side of the transect (low x axis values) corresponds with the high-latitude Southern Hemisphere, and the right side of the transect (high x axis values) corresponds with the high-latitude Northern Hemisphere. Note that map coordinates and the x-axis scale of the transect figures do not correspond to exact latitudes and longitudes because results were plotted on the CESM native grid (Figure 1).

In both the Atlantic and Pacific Ocean (Figures 6-9), the highest POC fluxes are found at the top of the water column because that is where POC is being generated through primary production. The highest amounts of POC flux are typically above the MLD_{max}, which can be most easily seen in the zoomed in transects (Figures 7 and 9). As in the depth profiles (Figure 5), flux attenuates at depth. In the Atlantic Ocean, the greatest declines in POC flux over the 21st century are seen in the North Atlantic, which also corresponds with the greatest shoaling of the MLD_{max} (Figure 6 and 7). It is important to note that this decline, though greatest at the surface, extends throughout the entire water column. Not only does this reduce the amount of carbon the ocean is able to store on long time scales, it also reduces the supply of energy to mesopelagic ecosystems, which rely on POC flux as the base of their food web (Cavan et al., 2019; Dall'Olmo et al., 2016).

One thing that is interesting to note about both the Atlantic and Pacific transects is that both show POC flux increases in Southern Hemisphere high-latitude regions, i.e. the Southern Ocean (Figures 6-9). As discussed earlier, this is likely related to increases in primary productivity in this region (Cabré et al., 2015; Laufkötter et al., 2015). Overall, the Atlantic Ocean transect shows greater magnitudes of simulated changes in POC flux, both in North Atlantic increases and Southern Ocean decreases, than are found in the Pacific Ocean transect. Viewing the depth resolved data as latitudinal transects highlights the relationship between regions of high POC flux and spatial variations in the MLD_{max}, which can be used to identify areas of high sequestration that would not be fully captured if only viewing POC flux at 100 m. For example, in the Equatorial Pacific (Figure 9a and b; lat = ~200) we see high rates of POC flux extending from the surface to below the MLD_{max} area with a shallow MLD_{max}, indicating that high rates of POC being sequestered long-term. In the North Atlantic, the transects provide a way of visualizing the scale of change and how this could relate to the massive shoaling of the MLD_{max} in this region (Figure 7). Declining POC flux could be the result of lower primary productivity in the North Atlantic surface ocean, a decrease in particle sinking speed, an increase in remineralization rates, or a combination of all of these factors. In more stratified water columns, particles do not have to sink as far to be sequestered long-term, yet in the North Atlantic we see MLD_{max} shoaling paired with large declines in POC flux, which indicates a strong decrease in carbon sequestration by the biological pump in this region. As a whole, and in the North Atlantic especially, the latitudinal transects reveal an overall decline in the biological pump's strength over the 21st century. Though there are some latitudes where POC flux increases over time, particularly in the Southern Ocean, these are outweighed by the regions of declining POC flux. Globally, this reflects what other model studies have predicted, that the

biological pump's strength will decrease as the result of a high emissions climate change scenario (Bopp et al. 2013; Cabré et al. 2015; Fu et al. 2016; Laufkötter et al. 2016; Palevsky and Doney 2021).

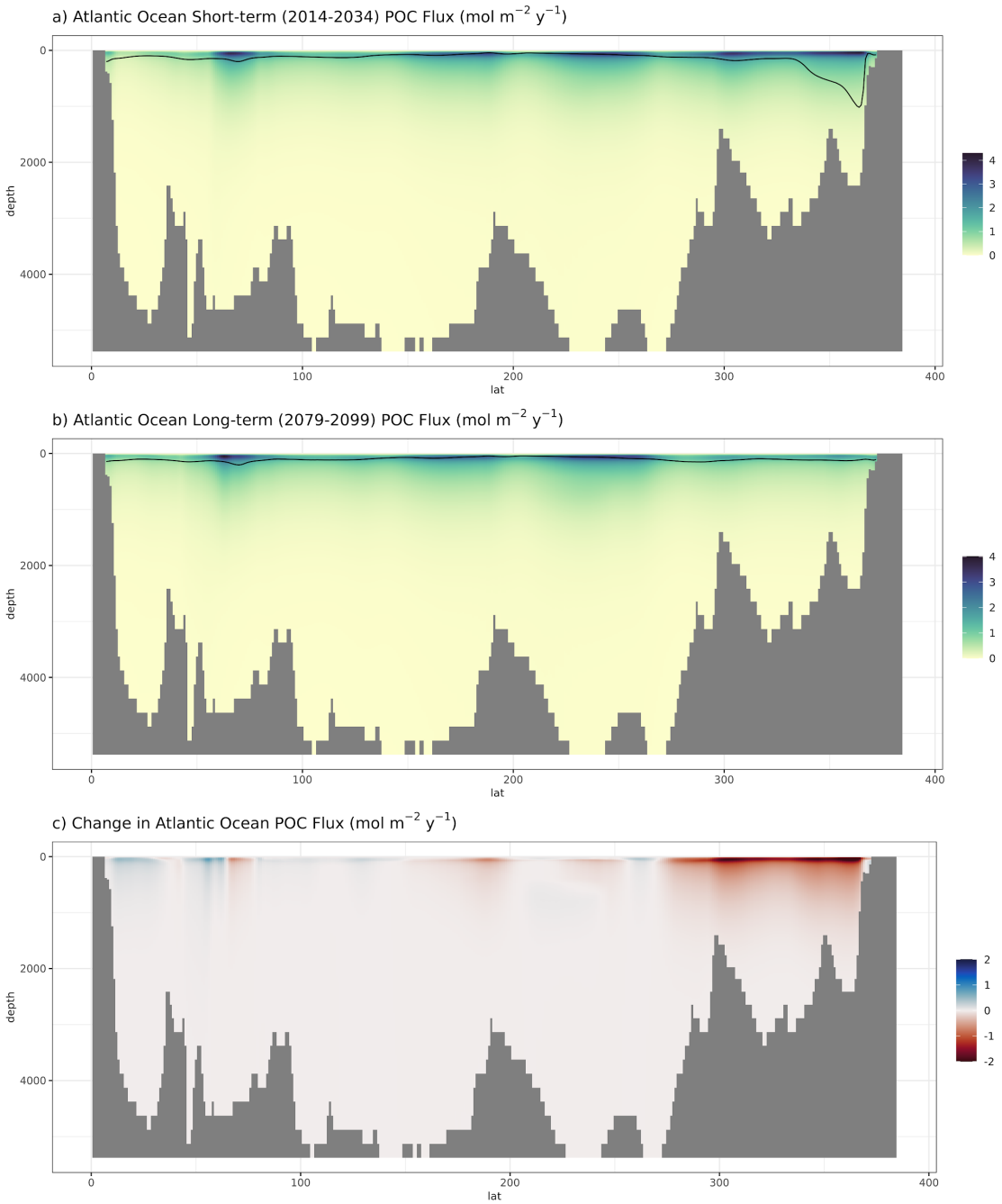

Figure 6. *Latitudinal transect of a) Short-term (2014-2034), b) Long-term (2079-2099), and c) Change in POC flux in the Atlantic Ocean throughout the entire water column. Results are plotted on the CESM native grid, thus a latitude of 0 corresponds with high-latitude Southern Hemisphere, and a latitude of 384 corresponds with high-latitude Northern Hemisphere. The black line in panels a and b indicates the maximum annual MLD, and all gray spaces are model grid cells outside the spatial domain of the marine biogeochemical model component. The exact Atlantic Ocean transect location is given in Figure 2.*

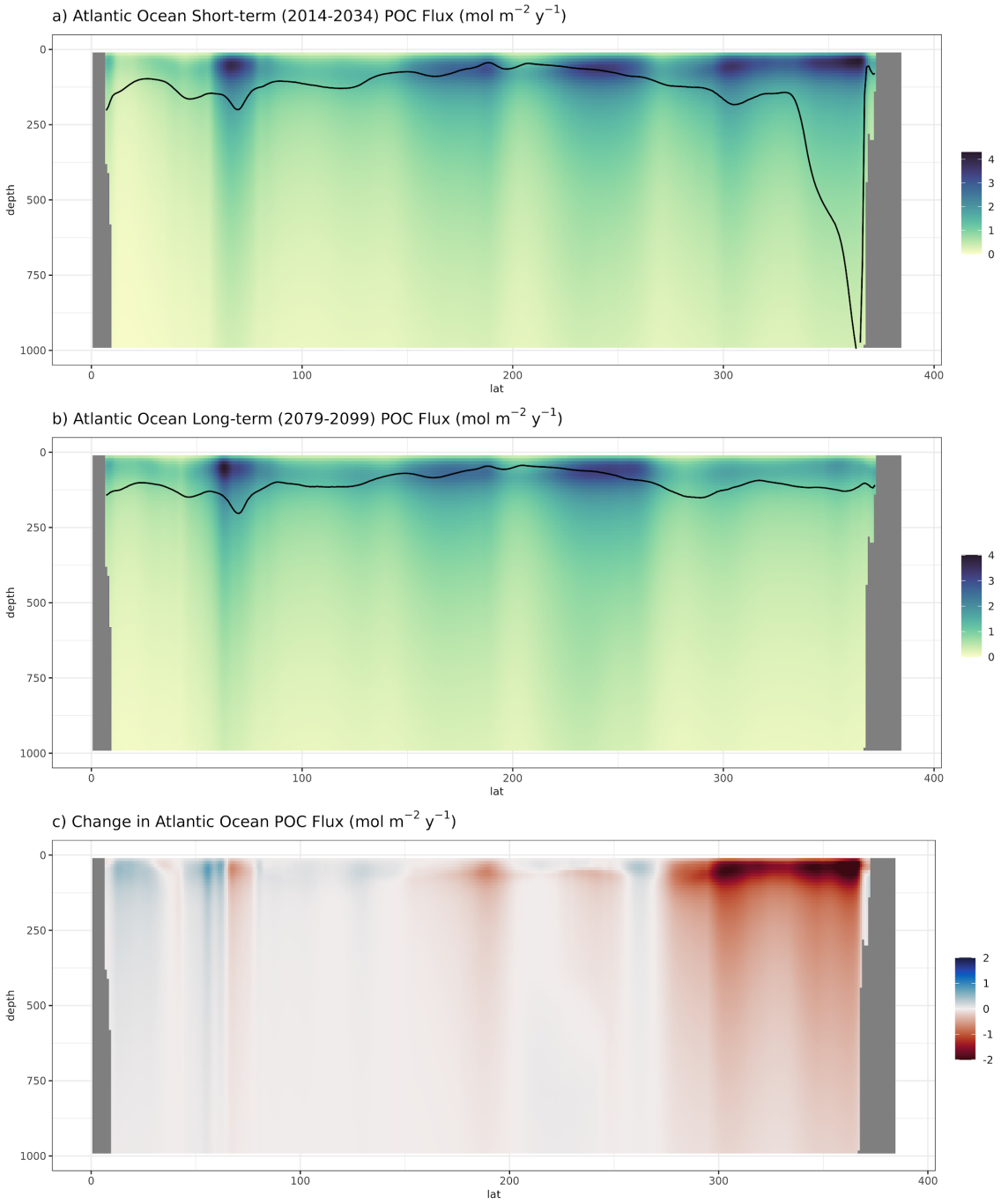

s

Figure 7. *Latitudinal transect of a) Short-term (2014-2034), b) Long-term (2079-2099), and c) Change in POC flux in the Atlantic Ocean zoomed in to 1000 m depth. Results are plotted on the CESM native grid, thus a latitude of 0 corresponds with high-latitude Southern Hemisphere, and a latitude of 384 corresponds with high-latitude Northern Hemisphere. The black line in panels a and b indicates the maximum annual MLD, and all gray spaces are model grid cells outside the spatial domain of the marine biogeochemical model component. The exact Atlantic Ocean transect location is given in Figure 2.*

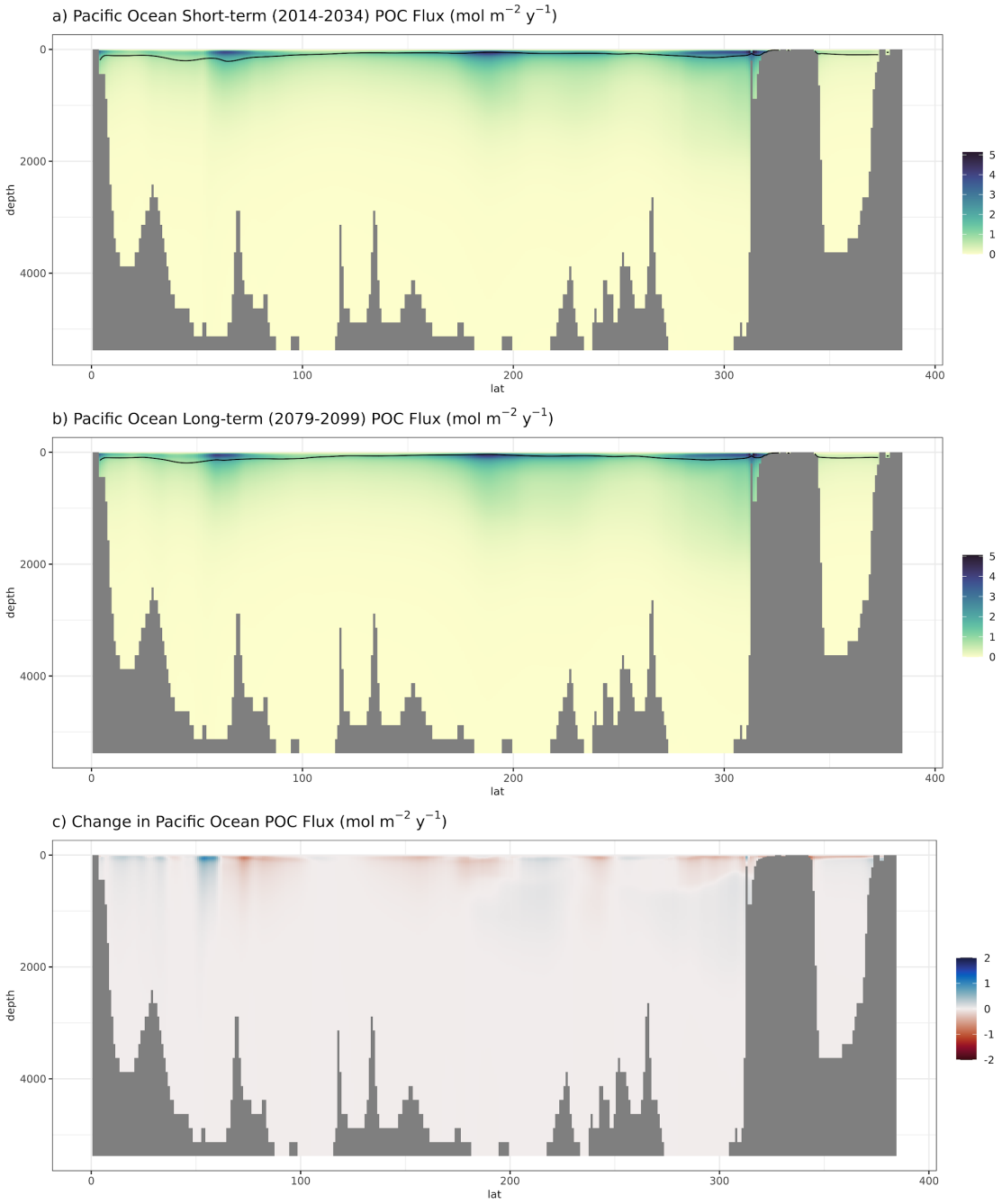

Figure 8. *Latitudinal transect of a) Short-term (2014-2034), b) Long-term (2079-2099), and c) Change in POC flux in the Pacific Ocean throughout the entire water column. Results are plotted on the CESM native grid, thus a latitude of 0 corresponds with high-latitude Southern Hemisphere, and a latitude of 384 corresponds with high-latitude Northern Hemisphere. The black line in panels a and b indicates the maximum annual MLD, and all gray spaces are model grid cells outside the spatial domain of the marine biogeochemical model component. The exact Pacific Ocean transect location is given in Figure 2.*

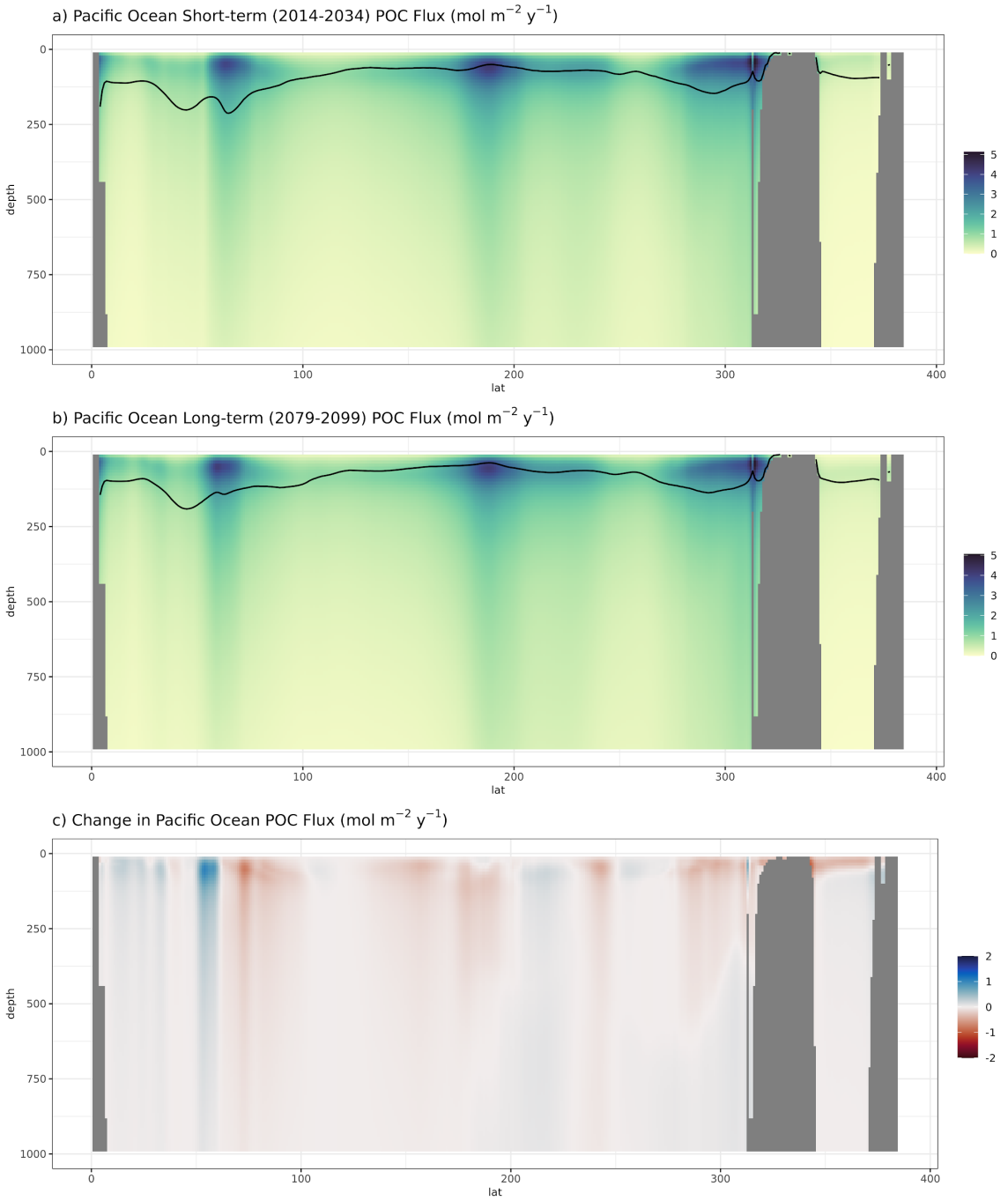

Figure 9. *Latitudinal transect of a) Short-term (2014-2034), b) Long-term (2079-2099), and c) Change in POC flux in the Pacific Ocean zoomed in to 1000 m depth. Results are plotted on the CESM native grid, thus a latitude of 0 corresponds with high latitude Southern-Hemisphere, and a latitude of 384 corresponds with high-latitude Northern Hemisphere. The black line in panels a and b indicates the maximum annual MLD, and all gray spaces are model grid cells outside the spatial domain of the marine biogeochemical model component. The exact Pacific Ocean transect location is given in Figure 2.*

Chapter 4: Conclusions and Future Research

4.1 Results summary

In summary, CESM data from a high-emissions scenario (SSP5-8.5) for the 21st century projects a 4.4% global decline in the strength of the biological pump, evaluated as POC flux through the 100 m depth horizon, though this decline is less severe than the predicted decline in the CMIP5 version of CESM (8.6%; Palevsky & Doney, 2021). Changes in POC flux are not distributed equally throughout the ocean; the greatest declines are found in the North Atlantic, the greatest increases are found in the Southern Ocean, and lower magnitudes of change are generally found in the subtropical gyres (Figure 3c). One key influence on changes in carbon sequestration by the biological pump are changes in the MLD_{max}, which is anticipated to shoal globally over the 21st century. Increased stratification, as we see most dramatically in the North Atlantic (Figure 4c), reduces nutrient supply and causes POC declines, but it could also mean that more POC is sequestered and not ventilated to the atmosphere through convective winter mixing. Thus, understanding POC flux patterns using depth resolved data gives a fuller picture of how POC flux is sequestered long-term than POC flux data archived solely at 100 m. In the six depth profile locations highlighted in this thesis (Figure 5), we see the maximum POC flux occurring in the surface ocean, and flux attenuation with depth. Flux magnitude, the extent of change, and the percent of POC flux that is occurring at various depths varies by location (Table 2). Latitudinal variations are also seen in POC flux across depth, as visualized through transects (Figures 6-9). CESM shows greater POC flux change in the Atlantic transect than the Pacific transect, with increases in Southern Hemisphere high-latitudes and decreases in most other areas, particularly in the North Atlantic. Declines in the strength of the biological pump will decrease

the ocean's ability to absorb CO_2 from the atmosphere, which could serve as a positive feedback exacerbating climate change.

4.2 Key contributions

My research contributes to ongoing conversations about using modeling to understand the biological pump and the impacts that climate change could have on this complex, biologically, and physically influenced system. It highlights the increased potential methods of analysis that are possible with CMIP6 data, in particular, the benefits of archived depth-resolved POC flux data, which was, for the first time, a priority variable to archive in CMIP6 (Orr et al. 2017). An additional key contribution from my thesis are the depth-resolved latitudinal transects that show the change in POC flux over the 21st century (Figures 6-9). Visualizing latitudinal patterns allows us to cross-compare modeled POC flux changes between ocean basins and helps us see how deep signals of POC flux change go. These latitudinal transects illustrate the importance of looking not just at the 100 m depth horizon, but at the full depth-resolved data. Variations in transfer efficiency and flux attenuation occur both spatially and over time in the modeled simulation, meaning that you cannot accurately understand the process of the biological pump just from 100 m.

My methodology demonstrates the benefits of cloud computing in ESM data analysis. Working with depth-resolved POC flux data adds 60 times as many data points to already large NetCDF files, which requires a computational capacity that scientists have not had to use in their previous analyses of ESM data. This can create an analysis barrier for scientists who don't have experience with or access to high-power virtual machines. Though it requires more background knowledge and can be very difficult at times (even with Microsoft Azure's relatively

user-friendly interface), cloud computing makes computational capacity less of an issue because I can resize my virtual machine to any level of computational power I need (Copeland et al., 2015). This is a major benefit when looking at large four dimensional ESM data because the virtual machine processes data much faster and does not crash. Furthermore, the process of downloading is much more efficient because the virtual machine runs using Microsoft's high-speed WiFi. This cloud computing methodology will be very useful in completing a multi-model comparison and being able to make more complex calculations using CESM data.

4.3 Additional modes of analysis

With the time spent learning the ins-and-outs of cloud computing, building my virtual machine, and acquiring all the necessary data, the scope of this thesis did not include enough time to complete a multi-model comparison between ESMs or analyze all the data that was of interest from the CESM2 simulation. Thus, I would like to outline additional analyses that would be useful to complete using the CESM2 data.

I chose to analyze data from the SSP5-8.5 scenario because, as the scenario with the highest levels of anthropogenic fossil fuel emissions and land use changes (O'Neill et al., 2016), it gives the strongest signals of climate change impacts on the Earth system. It is important to note that this study is more useful when interpreted as a process study, rather than a study solely about climate change predictions. I genuinely hope that the world does not have to deal with the impacts modeled in SSP5-8.5, both biological pump-related and otherwise. One thing that would be interesting and important to look at in the future are the impacts of climate change on the biological pump under more sustainable climate change scenarios, such as SSP1-2.6 or SSP2-4.5. This would give a better understanding of the range of impacts on the biological

pump, and would allow for further understanding of whether climate change impacts the biological pump linearly or nonlinearly.

The main additional calculation I would like to make on the CESM2 SSP5-8.5 data analyzed here is calculating POC flux at the MLD_{max} depth horizon, as seen in Palevsky & Doney (2021) and Palevsky & Doney (2018). For global and regional analyses related to the ocean's role as a carbon sink, MLD_{max} is the ideal depth horizon choice because below the MLD_{max}, POC is considered sequestered away from contact with the atmosphere on timescales longer than a year (Palevsky & Doney, 2018; Palevsky & Doney, 2021). POC that is sequestered below the shallower summer mixed layer depth may be vented and remineralized during times of convective winter mixing (Körtzinger et al., 2008; Palevsky et al., 2016), making the 100 m depth horizon, which is widely-used by modeling groups for its simplicity in calculating, less relevant for understanding the impact of POC flux on global climate. I anticipate that future analysis of the change in POC flux over the 21st century at the MLD_{max} depth horizon will show a slight decrease in the percent change of global carbon export as compared to the analysis at the 100 m depth horizon presented here, as this is what Palevsky and Doney (2021) found in their analysis of CESM1. I also expect more pronounced regional differences in POC flux change, particularly in the North Atlantic, where there is massive shoaling of the MLD_{max}.

Two additional variables I would like to investigate with the CESM2 data are net primary productivity (NPP) and the e-ratio, the fraction of NPP that is exported past the defined depth horizon. Globally, NPP is projected to decrease due in part to increased stratification, which inhibits the delivery of nutrients necessary for photosynthesis to the surface ocean, and increased warming-induced increases in grazing pressure (Laufkötter et al., 2015). However, in the Southern Ocean and Equatorial East Pacific, NPP is projected to increase due to mechanisms that

are not yet well understood (Laufkötter et al., 2016). E-ratio is predicted to decrease globally by 5.6% at the 100 m depth horizon in CESM1 (Palevsky & Doney, 2021), so I anticipate the e-ratio results in CESM2 will be similar. Additionally, I would like to investigate the change in e-ratio at both the 100 m depth horizon and the MLD_{max} depth horizon. Like the evaluation of POC flux at the MLD_{max} there has yet to be a multi-model comparison of e-ratio evaluated at the MLD_{max}.

4.4 Multi-model comparison

A next step to build upon this thesis would be to complete a multi-model comparison, which involves analyzing data from multiple ESMs to capture the range of model variability, thus giving an improved understanding of model uncertainty and areas of model disagreement. Model uncertainty can be a result of 1) model parameterizations - different formulas used to constrain model variables, 2) unforced internal variability - the fact that future climate is uncertain simply as a result of the chaotic nature of Earth's climate system, and 3) scenario variability - lack of knowledge of future emissions patterns and the resultant changes in radiative forcing (Lehner et al., 2020). Past multi-model comparison studies of the biological pump using CMIP5 models and scenario RCP8.5 (analogous to SSP5-8.5) have shown similar ranges of projected 21st century decline in global POC flux in their CMIP5 multi-model comparisons: 1% to 12% in Laufkötter et al (2016), 6 to 16% Cabré et al. (2015), 7 to 18% in Bopp et al. (2013), and 7 to 18% in Fu et al. (2016). Each of these studies were only able to evaluate POC flux changes at the 100 m depth horizon since CMIP5 did not archive depth-resolved POC flux output. At this time, no multi-model comparisons on POC flux or e-ratio using the MLD_{max} depth horizon, or any other depth horizon, have been completed. I have identified five CMIP6 models that would be good contenders for a multi-model comparison of POC flux using alternative depth

horizons: CESM2, GFDL-ESM2, MPI-ESM1-2, UKESM1-0-LL, and IPSL-CM6A. Cross comparing these models at multiple depth horizons - including MLD_{max}, 100 m, the base of the euphotic zone, and the particle compensation depth (Palevsky and Doney 2018) - and different scenarios would provide new insights to see the range of biogeochemical model differences from the most advanced ESMs available at this time. This would also help identify strong areas of uncertainty in ESM biogeochemical models, which could provide further justifications of areas to focus on improving data collection.

4.5 Improving marine biogeochemical models

Ultimately, it is important to remember that no model is a perfect representation of the natural world, and a model is only as good as the data and equations behind it. Marine biogeochemical modeling is a relatively new and actively evolving area of climate model research. Some of the key areas of improvement needed with ocean biogeochemical models include advancing parameterizations of the ballasting of particles, more complex characterizations of phytoplankton physiology and ecology, improved inclusion of micronutrients like copper, zinc, and iron, and improved coupling between Earth system components and the ocean biogeochemistry component (Séférian et al., 2020). CESM2, like other ESMs, does not fully represent the biological pump and by no means has a perfect representation of the parts represented. For instance, gravitational POC flux is just one aspect of the biological pump; DOC flux, the eddy pump, the mixed layer pump, and convective mixing are additional aspects that influence the biological pump (Le Moigne, 2019), and these aspects will all be impacted by climate change. By collecting more observational data in understudied regions, we can continue to improve ESMs and create better predictions that will help further

understanding of biological pump complexities, as well as fuel policy recommendations for reducing emissions and ensuring that SSP5-8.5 does not become a reality.

References

Behrenfeld, M. J., O'Malley, R. T., Siegel, D. A., McClain, C. R., Sarmiento, J. L., Feldman, G. C., Milligan, A. J., Falkowski, P. G., Letelier, R. M., & Boss, E. S. (2006). Climate-driven trends in contemporary ocean productivity. *Nature*, *444*(7120), 752–755. https://doi.org/10.1038/nature05317

Bopp, L., Monfray, P., Aumont, O., Dufresne, J.-L., Le Treut, H., Madec, G., Terray, L., & Orr, J. C. (2001). Potential impact of climate change on marine export production. *Global Biogeochemical Cycles*, *15*(1), 81–99. https://doi.org/10.1029/1999gb001256

Bopp, L., Resplandy, L., Orr, J. C., Doney, S. C., Dunne, J. P., Gehlen, M., Halloran, P., Heinze, C., Ilyina, T., Séférian, R., Tjiputra, J., & Vichi, M. (2013). Multiple stressors of ocean ecosystems in the 21st century: projections with CMIP5 models. *Biogeosciences* , *10*, 6225–6245. https://doi.org/10.5194/bg-10-6225-2013

Boucher, O., Servonnat, J., Albright, A. L., Aumont, O., Balkanski, Y., Bastrikov, V., Bekki, S., Bonnet, R., Bony, S., Bopp, L., Braconnot, P., Brockmann, P., Cadule, P., Caubel, A., Cheruy, F., Codron, F., Cozic, A., Cugnet, D., D'Andrea, F., … Vuichard, N. (2020). Presentation and Evaluation of the IPSL‐CM6A‐LR Climate Model. *Journal of Advances in Modeling Earth Systems*, *12*(7), 1-52. https://doi.org/10.1029/2019MS002010

Boyd, P. W., Claustre, H., Levy, M., Siegel, D. A., & Weber, T. (2019). Multi-faceted particle pumps drive carbon sequestration in the ocean. *Nature*, *568*, 327–335. https://doi.org/10.1038/s41586-019-1098-2

Cabré, A., Marinov, I., & Leung, S. (2015). Consistent global responses of marine ecosystems to future climate change across the IPCC AR5 earth system models. *Climate Dynamics*, *45*(5), 1253–1280. https://doi.org/10.1007/s00382-014-2374-3

Cael, B. B., & Bisson, K. (2018). Particle Flux Parameterizations: Quantitative and Mechanistic Similarities and Differences. *Frontiers in Marine Science*, *5*, 395. https://doi.org/10.3389/fmars.2018.00395

Cavan, E. L., Laurenceau-Cornec, E. C., Bressac, M., & Boyd, P. W. (2019). Exploring the ecology of the mesopelagic biological pump. *Progress in Oceanography*, *176*, 1-15. https://doi.org/10.1016/j.pocean.2019.102125

Copeland, M., Soh, J., Puca, A., Manning, M., & Gollob, D. (2015). *Microsoft Azure: Planning, Deploying, and Managing Your Data Center in the Cloud*. Apress. https://learning.oreilly.com/library/view/microsoft-azure-planning/9781484210437/9781484210444_FM_1_Title.xhtml

Dall'Olmo, G., Dingle, J., Polimene, L., Brewin, R. J. W., & Claustre, H. (2016). Substantial energy input to the mesopelagic ecosystem from the seasonal mixed-layer pump. *Nature Geoscience*, *9*(11), 820–823. https://doi.org/10.1038/ngeo2818

Danabasoglu, G., Lamarque, J. ‐F, Bacmeister, J., Bailey, D. A., DuVivier, A. K., Edwards, J.,

Emmons, L. K., Fasullo, J., Garcia, R., Gettelman, A., Hannay, C., Holland, M. M., Large, W. G., Lauritzen, P. H., Lawrence, D. M., Lenaerts, J. T. M., Lindsay, K., Lipscomb, W. H., Mills, M. J., … Strand, W. G. (2020). The Community Earth System Model Version 2 (CESM2). *Journal of Advances in Modeling Earth Systems*, *12*(2), 1-35. https://doi.org/10.1029/2019MS001916

Doney, S. C., Fabry, V. J., Feely, R. A., & Kleypas, J. A. (2009). Ocean acidification: the other CO2 problem. *Annual Review of Marine Science*, *1*, 169–192. https://doi.org/10.1146/annurev.marine.010908.163834

Doney, S. C., Ruckelshaus, M., Duffy, J. E., Barry, J. P., Chan, F., English, C. A., Galindo, H. M., Grebmeier, J. M., Hollowed, A. B., Knowlton, N., Polovina, J., Rabalais, N. N., Sydeman, W. J., & Talley, L. D. (2012). Climate change impacts on marine ecosystems. *Annual Review of Marine Science*, *4*, 11–37. https://doi.org/10.1146/annurev-marine-041911-111611

Dunne, J.P. (2019).“GFDL’s Fourth Generation CM4.0 and ESM4.1.” Presented at the Geophysical Fluid Dynamics Laboratory Review. https://www.gfdl.noaa.gov/wp-content/uploads/2019/12/7_dunne_Final_CM4_ESM4.pdf

Eyring, V., Bony, S., Meehl, G. A., Senior, C. A., Stevens, B., Stouffer, R. J., & Taylor, K. E. (2016). Overview of the Coupled Model Intercomparison Project Phase 6 (CMIP6) experimental design and organization. *Geoscientific Model Development*, *9*, 1937–1958. https://doi.org/10.5194/gmd-9-1937-2016

Friedlingstein, P., O’Sullivan, M., Jones, M. W., Andrew, R. M., Hauck, J., Olsen, A., Peters, G. P., Peters, W., Pongratz, J., Sitch, S., Le Quéré, C., Canadell, J. G., Ciais, P., Jackson, R. B., Alin, S., Aragão, L. E. O. C., Arneth, A., Arora, V., Bates, N. R., … Zaehle, S. (2020). Global carbon budget 2020. *Earth System Science Data*, *12*(4), 3269–3340. https://doi.org/10.5194/essd-12-3269-2020

Frölicher, T. L., Fischer, E. M., & Gruber, N. (2018). Marine heatwaves under global warming. *Nature*, *560*, 360–364. https://doi.org/10.1038/s41586-018-0383-9

Fu, W., Randerson, J. T., & Moore, J. K. (2016). Climate change impacts on net primary production (NPP) and export production (EP) regulated by increasing stratification and phytoplankton community structure in the CMIP5 models. *Biogeosciences* , *13*(18), 5151–5170. https://doi.org/10.5194/bg-13-5151-2016

Gent, P. R., Danabasoglu, G., Donner, L. J., Holland, M. M., Hunke, E. C., Jayne, S. R., Lawrence, D. M., Neale, R. B., Rasch, P. J., Vertenstein, M., Worley, P. H., Yang, Z.-L., & Zhang, M. (2011). The Community Climate System Model Version 4. *Journal of Climate*, *24*(19), 4973–4991. https://doi.org/10.1175/2011JCLI4083.1

Gruber, N. (2011). Warming up, turning sour, losing breath: ocean biogeochemistry under global change. *Philosophical Transactions of the Royal Society Series A*, *369*, 1980–1996. https://doi.org/10.1098/rsta.2011.0003

Gutjahr, O., Putrasahan, D., Lohmann, K., Jungclaus, J. H., Storch, J.-S. von, Brüggemann, N.,

Haak, H., & Stössel, A. (2019). Max Planck Institute Earth System Model (MPI-ESM1.2) for the High-Resolution Model Intercomparison Project (HighResMIP). *Geoscientific Model Development*, *12*(7), 3241–3281. https://doi.org/10.5194/gmd-12-3241-2019

Hayhoe, K., Edmonds, J., Kopp, R., LeGrande, A., Sanderson, B., Wehner, M., & Wuebbles, D. (2017). *Climate models, scenarios, and projections*. Publications, Agencies and Staff of the U.S. Department of Commerce. https://digitalcommons.unl.edu/usdeptcommercepub/589

Heavens, N. G., Ward, D. S., & Natalie, M. M. (2013). *Studying and Projecting Climate Change with Earth System Models*. Nature Education Knowledge. https://www.nature.com/scitable/knowledge/library/studying-and-projecting-climate-change-with-earth-103087065/

Hurrell, J. W., Holland, M. M., Gent, P. R., Ghan, S., Kay, J. E., Kushner, P. J., Lamarque, J.-F., Large, W. G., Lawrence, D., Lindsay, K., Lipscomb, W. H., Long, M. C., Mahowald, N., Marsh, D. R., Neale, R. B., Rasch, P., Vavrus, S., Vertenstein, M., Bader, D., … Marshall, S. (2013). The Community Earth System Model: A Framework for Collaborative Research. *Bulletin of the American Meteorological Society*, *94*(9), 1339–1360. https://doi.org/10.1175/BAMS-D-12-00121.1

Jia, H., & Chong, A. (2021). *Package "epwshiftr"* (Version 0.1.2) [Computer software]. https://cran.r-project.org/web/packages/epwshiftr/epwshiftr.pdf

Jónasdóttir, S. H., Visser, A. W., Richardson, K., & Heath, M. R. (2015). Seasonal copepod lipid pump promotes carbon sequestration in the deep North Atlantic. *Proceedings of the National Academy of Sciences of the United States of America*, *112*(39), 12122–12126. https://doi.org/10.1073/pnas.1512110112

Juckes, M., Taylor, K. E., Durack, P. J., Lawrence, B., Mizielinski, M. S., Pamment, A., Peterschmitt, J.-Y., Rixen, M., & Sénési, S. (2020). The CMIP6 Data Request (DREQ, version 01.00.31). *Geosci. Model Dev.*, *13*, 201–224. https://doi.org/10.5194/gmd-13-201-2020

Karl, D. M., & Lukas, R. (1996). The Hawaii Ocean Time-series (HOT) program: Background, rationale and field implementation. *Deep-Sea Research. Part II, Topical Studies in Oceanography*, *43*(2), 129–156. https://doi.org/10.1016/0967-0645(96)00005-7

Körtzinger, A., Send, U., Lampitt, R. S., Hartman, S., Wallace, D. W. R., Karstensen, J., Villagarcia, M. G., Llinás, O., & DeGrandpre, M. D. (2008). The seasonal pCO_2 cycle at 49°N/16.5°W in the northeastern Atlantic Ocean and what it tells us about biological productivity. *Journal of Geophysical Research*, *113*, C04020. https://doi.org/10.1029/2007jc004347

Kwiatkowski, L., Torres, O., Bopp, L., Aumont, O., Chamberlain, M., Christian, J. R., Dunne, J. P., Gehlen, M., Ilyina, T., John, J. G., Lenton, A., Li, H., Lovenduski, N. S., Orr, J. C., Palmieri, J., Santana-Falcón, Y., Schwinger, J., Séférian, R., Stock, C. A., … Ziehn, T. (2020). Twenty-first century ocean warming, acidification, deoxygenation, and upper-ocean nutrient and primary production decline from CMIP6 model projections. *Biogeosciences* , *17*(13), 3439–3470. https://doi.org/10.5194/bg-17-3439-2020

Laufkötter, C., Vogt, M., Gruber, N., Aita-Noguchi, M., Aumont, O., Bopp, L., Buitenhuis, E., Doney, S. C., Dunne, J., Hashioka, T., Hauck, J., Hirata, T., John, J., Le Quéré, C., Lima, I. D., Nakano, H., Seferian, R., Totterdell, I., Vichi, M., & Völker, C. (2015). Drivers and uncertainties of future global marine primary production in marine ecosystem models. *Biogeosciences* , *12*(23), 6955–6984. https://doi.org/10.5194/bg-12-6955-2015

Laufkötter, C., Vogt, M., Gruber, N., Aumont, O., Bopp, L., Doney, S. C., Dunne, J. P., Hauck, J., John, J. G., Lima, I. D., Seferian, R., & Völker, C. (2016). Projected decreases in future marine export production: the role of the carbon flux through the upper ocean ecosystem. *Biogeosciences* , *13*(13), 4023–4047. https://doi.org/10.5194/bg-13-4023-2016

Lehner, F., Deser, C., Maher, N., Marotzke, J., Fischer, E. M., Brunner, L., Knutti, R., & Hawkins, E. (2020). Partitioning climate projection uncertainty with multiple large ensembles and CMIP5/6. *Earth System Dynamics*, *11*, 491–508. https://doi.org/10.5194/esd-11-491-2020

Le Moigne, F. A. C. (2019). Pathways of Organic Carbon Downward Transport by the Oceanic Biological Carbon Pump. *Frontiers in Marine Science*, *6(634)*, 1-8. https://doi.org/10.3389/fmars.2019.00634

Marsay, C. M., Sanders, R. J., Henson, S. A., Pabortsava, K., Achterberg, E. P., & Lampitt, R. S. (2015). Attenuation of sinking particulate organic carbon flux through the mesopelagic ocean. *Proceedings of the National Academy of Sciences of the United States of America*, *112*(4), 1089–1094. https://doi.org/10.1073/pnas.1415311112

Martin, J. H., Knauer, G. A., Karl, D. M., & Broenkow, W. W. (1987). VERTEX: carbon cycling in the northeast Pacific. *Deep-Sea Research. Part A, Oceanographic Research Papers*, *34*(2), 267–285. https://doi.org/10.1016/0198-0149(87)90086-0

Moore, J. K., Doney, S. C., & Lindsay, K. (2004). Upper ocean ecosystem dynamics and iron cycling in a global three-dimensional model. *Global Biogeochemical Cycles*, *18*(4), 1-21. https://doi.org/10.1029/2004gb002220

Moore, K., J, Lindsay, K., Doney, S. C., Long, M. C., & Misumi, K. (2013). Marine Ecosystem Dynamics and Biogeochemical Cycling in the Community Earth System Model [CESM1(BGC)]: Comparison of the 1990s with the 2090s under the RCP4.5 and RCP8.5 Scenarios. *Journal of Climate*, *26*(23), 9291–9312. https://doi.org/10.1175/JCLI-D-12-00566.1

Morzaria-Luna, H. N. (2020). *Current Configuration Ubuntu Server 18.04 (Bionic Beaver) Repository*. Github. https://github.com/hmorzaria/atlantis_azure

O'Neill, B. C., Kriegler, E., Riahi, K., Ebi, K. L., Hallegatte, S., Carter, T. R., Mathur, R., & van Vuuren, D. P. (2014). A new scenario framework for climate change research: the concept of shared socioeconomic pathways. *Climatic Change*, *122*, 387–400. https://doi.org/10.1007/s10584-013-0905-2

O'Neill, B. C., Tebaldi, C., van Vuuren, D. P., Eyring, V., Friedlingstein, P., Hurtt, G., Knutti, R., Kriegler, E., Lamarque, J.-F., Lowe, J., Meehl, G. A., Moss, R., Riahi, K., & Sanderson, B.

M. (2016). The Scenario Model Intercomparison Project (ScenarioMIP) for CMIP6. *Geoscientific Model Development*, *9*, 3461–3482. https://doi.org/10.5194/gmd-9-3461-2016

Orr, J. C., Najjar, R. G., Aumont, O., Bopp, L., Bullister, J. L., Danabasoglu, G., Doney, S. C., Dunne, J. P., Dutay, J.-C., Graven, H., Griffies, S. M., John, J. G., Joos, F., Levin, I., Lindsay, K., Matear, R. J., McKinley, G. A., Mouchet, A., Oschlies, A., … Yool, A. (2017). Biogeochemical protocols and diagnostics for the CMIP6 Ocean Model Intercomparison Project (OMIP). *Geoscientific Model Development*, *10*(6), 2169–2199. https://doi.org/10.5194/gmd-10-2169-2017

Oschlies, A., Schulz, K. G., Riebesell, U., & Schmittner, A. (2008). Simulated 21st century's increase in oceanic suboxia by CO2-enhanced biotic carbon export. Global Biogeochemical Cycles, *22*(4), 1–10. https://doi.org/10.1029/2007GB003147

Oschlies, A., Brandt, P., Stramma, L., & Schmidtko, S. (2018). Drivers and mechanisms of ocean deoxygenation. *Nature Geoscience*, *11*(7), 467–473. https://doi.org/10.1038/s41561-018-0152-2

Palevsky, H. I., & Doney, S. C. (2018). How choice of depth horizon influences the estimated spatial patterns and global magnitude of ocean carbon export flux. *Geophysical Research Letters*, *45*(9), 4171–4179. https://doi.org/10.1029/2017gl076498

Palevsky, H. I., & Doney, S. C. (2021). Sensitivity of 21st century ocean carbon export flux projections to the choice of export depth horizon. *Global Biogeochemical Cycles*, *35*(2). https://doi.org/10.1029/2020gb006790

Palevsky, H. I., & Nicholson, D. P. (2018). Insights from the Ocean Observatories Initiative Irminger Sea Array. *Oceanography* , *31*(1), 42–49. https://doi.org/10.2307/26307786

Palevsky, H. I., Quay, P. D., Lockwood, D. E., & Nicholson, D. P. (2016). The annual cycle of gross primary production, net community production, and export efficiency across the North Pacific Ocean. *Global Biogeochemical Cycles*, *30*(2), 361–380. https://doi.org/10.1002/2015gb005318

Parekh, P., Dutkiewicz, S., Follows, M. J., & Ito, T. (2006). Atmospheric carbon dioxide in a less dusty world. *Geophysical Research Letters*, *33*(3), 1-4. https://doi.org/10.1029/2005gl025098

Rew, R., & Davis, G. (1990). NetCDF: an interface for scientific data access. *IEEE Computer Graphics and Applications*, *10*(4), 76–82. https://doi.org/10.1109/38.56302

Riahi, K., van Vuuren, D. P., Kriegler, E., Edmonds, J., O'Neill, B. C., Fujimori, S., Bauer, N., Calvin, K., Dellink, R., Fricko, O., Lutz, W., Popp, A., Cuaresma, J. C., Kc, S., Leimbach, M., Jiang, L., Kram, T., Rao, S., Emmerling, J., … Tavoni, M. (2017). The Shared Socioeconomic Pathways and their energy, land use, and greenhouse gas emissions implications: An overview. *Global Environmental Change: Human and Policy Dimensions*, *42*, 153–168. https://doi.org/10.1016/j.gloenvcha.2016.05.009

Sallée, J.-B., Pellichero, V., Akhoudas, C., Pauthenet, E., Vignes, L., Schmidtko, S., Garabato, A.

N., Sutherland, P., & Kuusela, M. (2021). Summertime increases in upper-ocean stratification and mixed-layer depth. *Nature*, *591*, 592–598. https://doi.org/10.1038/s41586-021-03303-x

Séférian, R., Berthet, S., Yool, A., Palmiéri, J., Bopp, L., Tagliabue, A., Kwiatkowski, L., Aumont, O., Christian, J., Dunne, J., Gehlen, M., Ilyina, T., John, J. G., Li, H., Long, M. C., Luo, J. Y., Nakano, H., Romanou, A., Schwinger, J., … Yamamoto, A. (2020). Tracking Improvement in Simulated Marine Biogeochemistry Between CMIP5 and CMIP6. *Current Climate Change Reports*, *6*, 95-119. https://doi.org/10.1007/s40641-020-00160-0

Sellar, A. A., Jones, C. G., Mulcahy, J. P., Tang, Y., Yool, A., Wiltshire, A., O'Connor, F. M., Stringer, M., Hill, R., Palmieri, J., Woodward, S., Mora, L., Kuhlbrodt, T., Rumbold, S. T., Kelley, D. I., Ellis, R., Johnson, C. E., Walton, J., Abraham, N. L., … Zerroukat, M. (2019). UKESM1: Description and Evaluation of the U.K. Earth System Model. *Journal of Advances in Modeling Earth Systems*, *11*(12), 4513–4558. https://doi.org/10.1029/2019MS001739

Semenov, M. A., & Stratonovitch, P. (2010). Use of multi-model ensembles from global climate models for assessment of climate change impacts. *Climate Research*, *41*(1), 1–14. https://doi.org/10.3354/cr00836

Siegel, D. A., Buesseler, K. O., Doney, S. C., Sailley, S. F., Behrenfeld, M. J., & Boyd, P. W. (2014). Global assessment of ocean carbon export by combining satellite observations and food-web models. *Global Biogeochemical Cycles*, *28*(3), 181–196. https://doi.org/10.1002/2013gb004743

Smith, L. M., Barth, J. A., Kelley, D. S., Plueddemann, A., Rodero, I., Ulses, G. A., Vardaro, M. F., & Weller, R. (2018). The Ocean Observatories Initiative. *Oceanography* , *31*(1), 16–35. http://www.jstor.org/stable/26307783

Smith, R., Jones, P., Briegleb, B., Bryan, F., Danabasoglu, G., Dennis, J., Dukowicz, J., Eden, C., Fox-Kemper, B., Gent, P., Hecht, M., Jayne, S., Jochum, M., Large, W., Lindsay, K., Maltrud, M., Norton, N., Peacock, S., Vertenstein, M., & Yeager, S. (2010). *The Parallel Ocean Program (POP) Reference Manual* (Version 2). https://www.cesm.ucar.edu/models/cesm1.0/pop2/doc/sci/POPRefManual.pdf

Steinberg, D. K., Carlson, C. A., Bates, N. R., Johnson, R. J., Michaels, A. F., & Knap, A. H. (2001). Overview of the US JGOFS Bermuda Atlantic Time-series Study (BATS): a decade-scale look at ocean biology and biogeochemistry. *Deep-Sea Research. Part II, Topical Studies in Oceanography*, *48*(8), 1405–1447. https://doi.org/10.1016/S0967-0645(00)00148-X

Tebaldi, C., Debeire, K., Eyring, V., Fischer, E., Fyfe, J., Friedlingstein, P., Knutti, R., Lowe, J., O'Neill, B., Sanderson, B., van Vuuren, D., Riahi, K., Meinshausen, M., Nicholls, Z., Hurtt, G., Kriegler, E., Lamarque, J.-F., Meehl, G., Moss, R., … Ziehn, T. (2020). Climate model projections from the Scenario Model Intercomparison Project (ScenarioMIP) of CMIP6. *Earth System Dynamics, 12*, 253-293. https://doi.org/10.5194/esd-12-253-2021

Walker, S. (2020). *Puget Sound Downscaling Repository* [Github].

https://github.com/steviewalker/Puget_Sound_Downscaling

Walker, S., Morzaria Luna, H. N., Kaplan, I., & Petatán-Ramírez, D. (2021). Future temperature and salinity in Puget Sound, Washington State, under CMIP6 climate change scenarios. *Manuscript submitted for publication*.